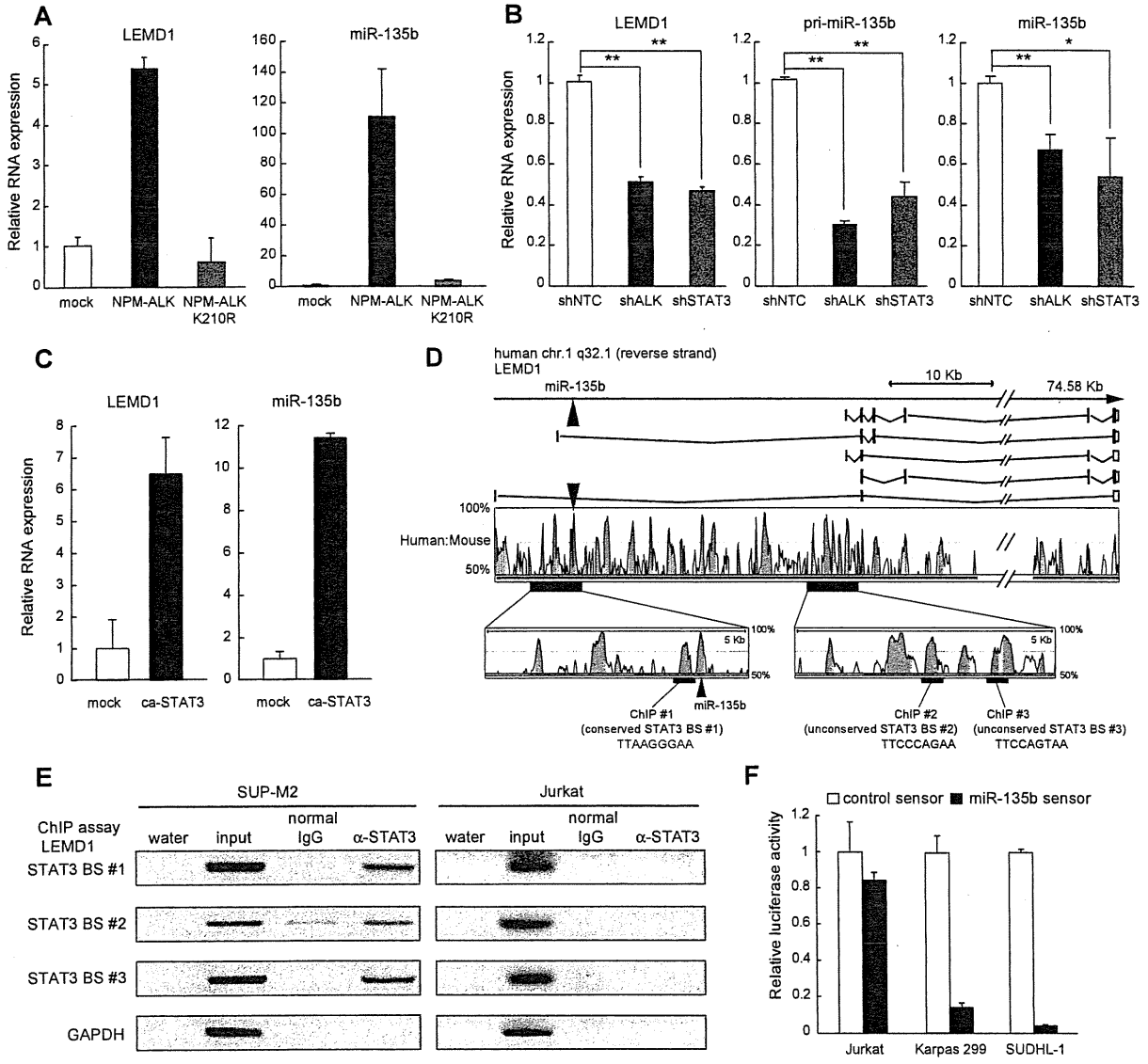

Figure 2. Identification of NPM-ALK-STAT3-miR-135b axis in ALCL. (A) Induction of LEMD1/miR-135b by NPM-ALK. Jurkat cells were transduced with lentivirus carrying NPM-ALK or kinase-dead NPM-ALK (K210R) and subjected to qRT-PCR analysis. (B) NPM-ALK/STAT3–dependent up-regulation of LEMD1/miR-135b in ALCL. Effects of shRNAs against NPM-ALK and STAT3 were evaluated in SUDHL-1 cells (*$P < .05$; **$P < .01$). (C) Up-regulation of LEMD1/miR-135b by ca-STAT3. Jurkat cells were transduced with lentivirus carrying mouse ca-STAT3 and subjected to qRT-PCR analysis. (D) STAT3 binding sites in *LEMD1* genomic region. Top panel indicates schematic genomic organization of human *LEMD1* gene and miR-135b. Sequence conservation between human and mouse is represented as the percentage of conservation in the Vista analysis shown in the middle panel. We analyzed putative STAT3-binding sites within the conserved region in ChIP analysis, and we found that STAT3 bound to 3 sites in the bottom panel, as shown in panel E. Number 1 site (TTAAGGGAA) is conserved between human and mouse. (E) Binding of STAT3 to LEMD1 genomic regions analyzed by ChIP analysis in SUP-M2 (left) and Jurkat (right) cells. Total chromatin before immunoprecipitation was used as positive control for PCR. Jurkat cells were used as negative control. (F) Enhanced miR-135b activity in ALCL. Cells were transfected with miRNA sensor vectors and applied to luciferase assay. Reflecting high miR-135b expression, luciferase expression levels from miR-135b sensor vector were remarkably lower than those from control sensor vector in ALCL cells but not in Jurkat cells.

Figure 2A-B). To identify the endogenous and functional target(s) of miR-135b in ALCL cells, we achieved the efficient long-term suppression of miR-135b activity through the decoy RNA system, in which RNA decoys against specific miRNA (TuD RNA) are driven by RNA polymerase III (Figure 3A).[11] Introduction of TuD RNA indeed strongly inhibited miR-135b activity in ALCL cell lines (Figure 3B-C and supplemental Figure 2C-D).

Using this system, we consequently identified FOXO1 as an endogenous target of miR-135b in ALCL (Figure 3D-G). The FOXO1 3′UTR contains a potential miR-135b–binding site and exogenous miR-135b suppressed FOXO1 protein expression and its translational efficiency depending on the target site, clarifying FOXO1 as a novel target of miR-135b (Figure 3D-F). Knockdown of miR-135b increased the protein expression of FOXO-dependent cell cycle inhibitors p21 and p27 as well as FOXO1 itself in ALCL cells (Figure 3G and supplemental Figure 2E). In Karpas 299 cells containing a barely detectable FOXO1, miR-135b suppression up-regulated p27 and alternatively another positive regulator of p27, CREG1 (supplemental Figure 2E).[20] Considering that NPM-ALK has been shown to inhibit FOXO3a activity through FOXO3a phosphorylation by AKT activation,[21] NPM-ALK might thus regulate a wide range of FOXO family activities via protein modification and posttranscriptional regulation. Because FOXO factors are critical mediators in growth inhibitory responses to

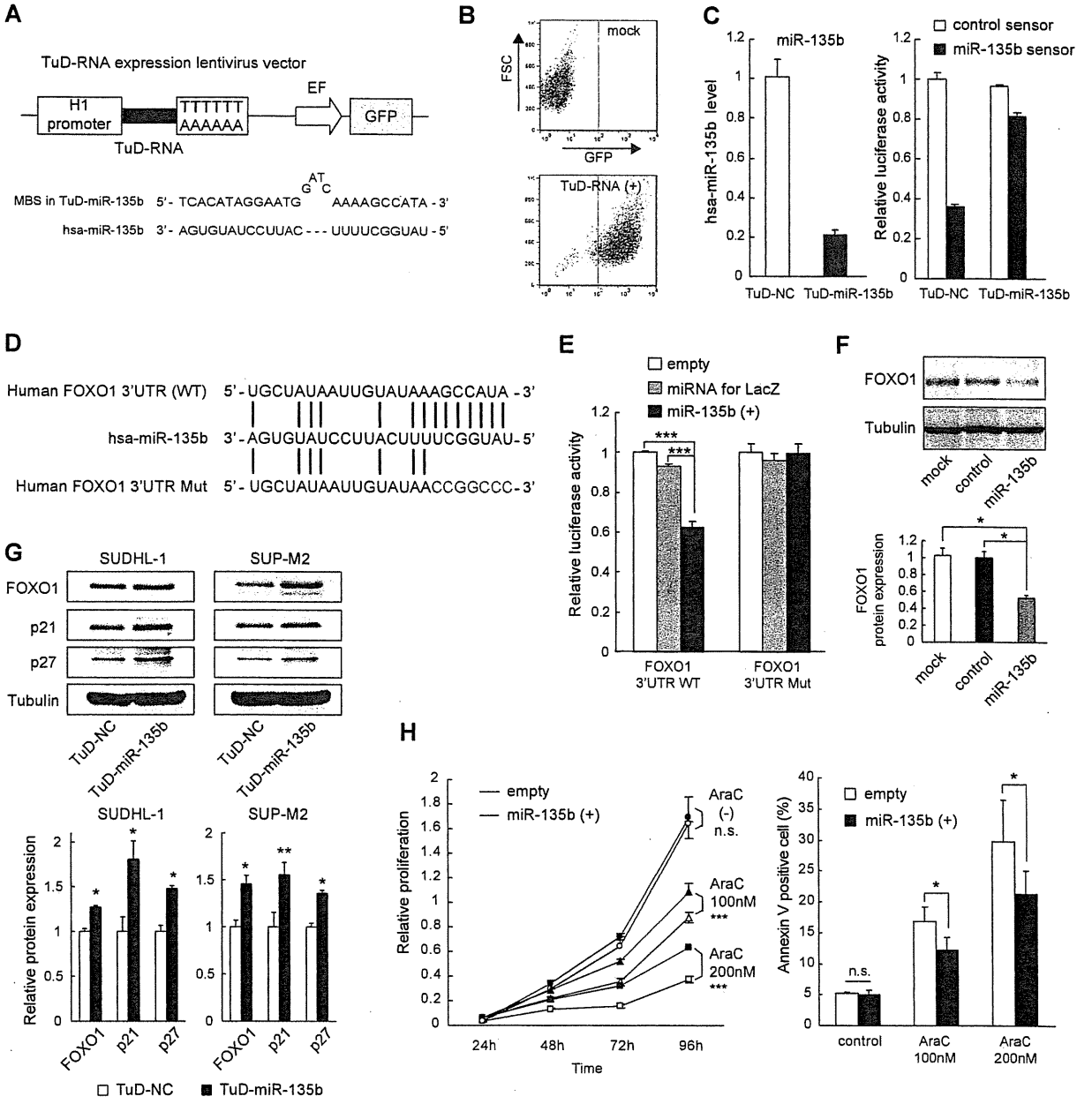

Figure 3. miR-135b targets FOXO1 and regulates chemosensitivity. (A) Structure of TuD RNA expression vector. TuD RNA for miR-135b contains miRNA-binding site (MBS) that is partially complementary to miR-135b. Details of TuD RNA structure have been described previously.[11] (B) Introduction of TuD RNA against miR-135b into ALCL cells. Flow cytometry profiles indicating transduction efficiency in Karpas 299 cells. FSC indicates forward scatter. (C) Inhibition of miR-135b function by TuD RNA for miR-135b. Left and right panels show qRT-PCR result and luciferase assay monitoring miR-135b activity, respectively. NC indicates negative control. (D) Sequence alignment between miR-135b and its putative binding site in the FOXO1 3'UTR. (E) miR-135b targets FOXO1. HEK293T cells were transfected with luciferase reporter containing the FOXO1 3'UTR with wild-type or mutated target site (shown in panel D), along with empty vector, miRNA-lacZ expression control vector (miRNA for lacZ), or pri-miR-135b expression vector [miR-135b (+)]. Luciferase assay was performed 48 hours after transfection (***$P < .001$). (F) Suppression of FOXO1 protein level by miR-135b. HeLa cells were transiently transfected with miR-135b and subjected to immunoblot analysis. (G) Elevated expression of FOXO1, p21, and p27 by miR-135b inhibition in ALCL cells. SUDHL-1 and SUP-M2 cells were infected with lentivirus harboring TuD-NC or TuD-miR-135b and applied to immunoblot analysis. The quantification results were shown in the bottom panel. (H) miR-135b–mediated attenuation of chemosensitivity. Jurkat cells with empty or pri-miR-135b vectors were treated with cytosine β-D-arabinofuranoside (AraC), followed by the assessment of cell viability (left) and apoptosis (right; *$P < .05$; ***$P < .001$; n.s., not significant).

various stresses, including DNA damage,[22] we examined the effect of miR-135b on the sensitivity to chemotherapeutic drugs to investigate functional consequences of FOXO1 alteration by miR-135b. Although miR-135 overexpression did not affect the proliferation of Jurkat cells under normal conditions, Jurkat cells overexpressing miR-135b were more resistant to cytosine β-D-arabinofuranoside (Figure 3H). These results suggest a possibility that miR-135b may confer chemoresistance to ALCL cells through FOXO1 modulation.

Targeting of Th2 regulators STAT6 and GATA3 by miR-135b

It was shown previously that constitutive activation of ALK chimeric proteins is sufficient to induce cellular transformation and

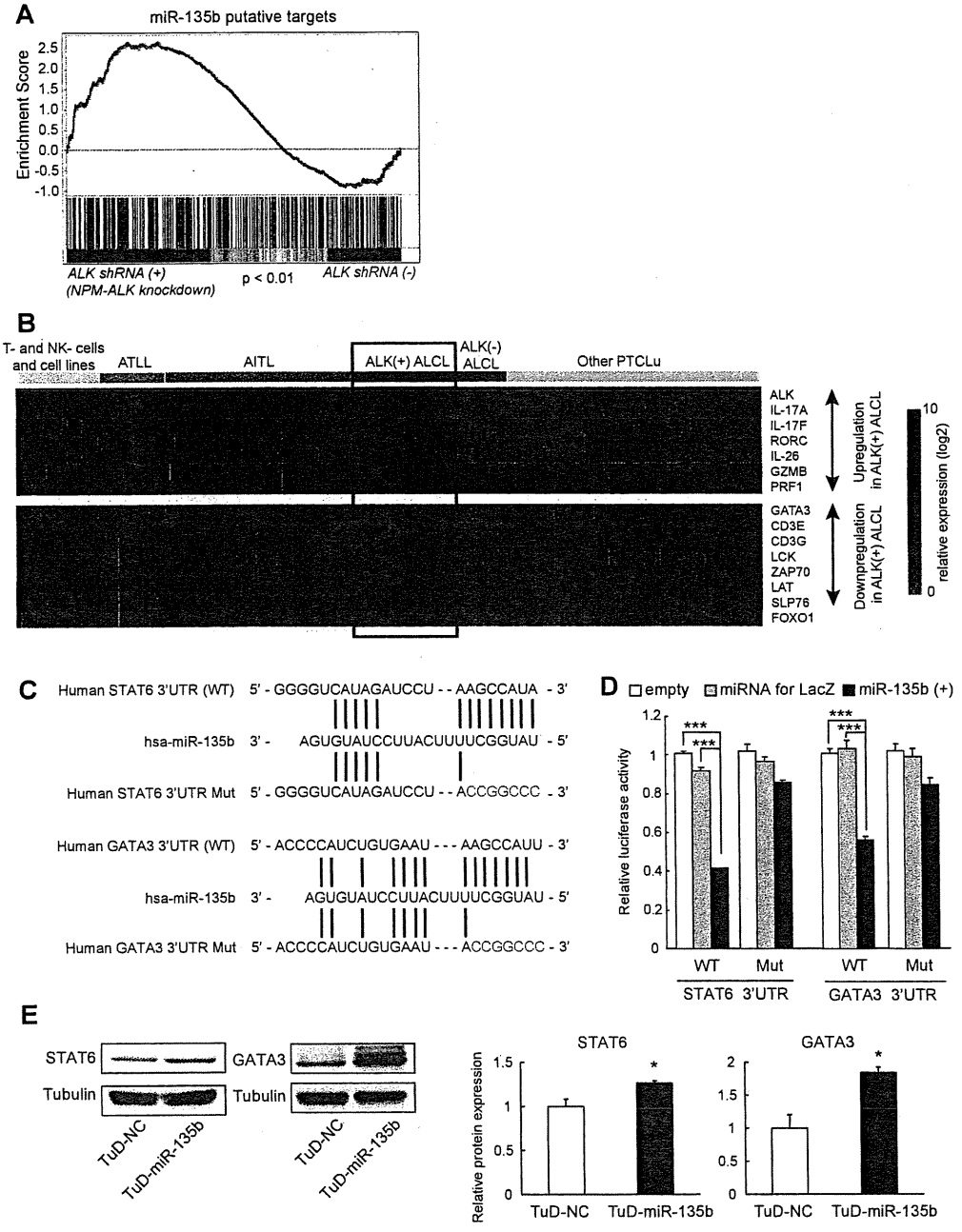

Figure 4. Targeting of STAT6 and GATA3 by miR-135b in ALCL. (A) Up-regulation of miR-135b target genes was evaluated on NPM-ALK knockdown using GSEA (dataset GSE6184). (B) Heat map showing the expression of Th17-related molecules, GATA3, FOXO1, and other ALCL-related genes (GZMB, PRF1, and TCR-related genes) in PTCL. Gene expression data are derived from GSE19069. In addition to GATA3, FOXO1 expression in ALCL was also lower than those in other PTCLs. ATLL indicates adult T-cell leukemia/lymphoma; AITL, angioimmunoblastic T-cell lymphoma; and PTCLu, PTCL-unclassifiable. (C) Sequence alignment between miR-135b and its putative binding sites in the STAT6 and GATA3 3′UTRs. (D) miR-135b targets STAT6 and GATA3. Luciferase activity of the STAT6 and GATA3 3′UTR reporter constructs with wild-type or mutated target site (shown in panel C) in HEK293T cells cotransfected with empty vector, miRNA-lacZ expression control vector (miRNA for lacZ), or pri-miR-135b expression vector [miR-135b (+)]; ***$P < .001$). (E) Up-regulation of STAT6 and GATA3 by TuD-RNA–mediated miR-135b inhibition in Karpas 299 cells. The quantification results were shown in the right panel.

that ALK activity is indispensable for the survival of ALK-positive ALCL cells.[9] In the pathogenesis of ALCL, ALK elicits reproducible transcriptome changes, as shown by previous GEP analysis.[12] To gain insight for overall interconnection between NPM-ALK–driven gene response and miR-135b–mediated gene regulation, we performed GSEA using the GEP results of ALCL cells with or without shRNA-mediated NPM-ALK inhibition.[12,16] GSEA demonstrated a significant up-regulation of miR-135b potential targets on NPM-ALK suppression, indicating that miR-135b constitutes an arm of multiple NPM-ALK downstream pathways (Figure 4A and supplemental Figure 3A). This approach suggested TGFBR1, SIRT1, cyclin G2, CREG1, Bcl11b, and STAT6 as additional candidate targets of the NPM-ALK–miR-135b pathway.

ALCL of T-lymphocyte origin has been known to present with a T- or null-cell phenotype and lack TCR complex-related molecules such as CD3ε and ZAP70, despite the presence of TCR rearrangements (Figure 4B).[23] Alternatively, recent GEP analysis in PTCL has demonstrated the following characters of ALCL cells: high

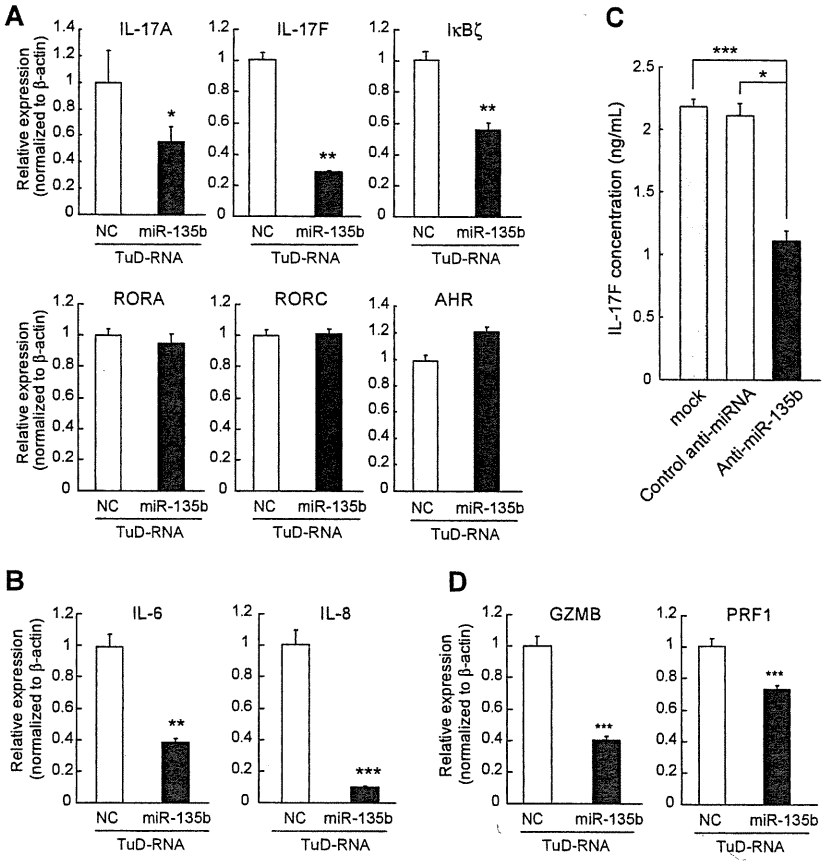

Figure 5. miR-135b blockade suppresses IL-17 production by ALCL cells and modulates ALCL immunophenotype. (A) Regulation of Th17-related molecules by miR-135b. Karpas 299 cells were infected with lentivirus harboring TuD-NC or TuD-miR-135b and applied to qRT-PCR analysis. Effects of miR-135b inhibition on the transcripts of Th17-related molecules were analyzed by qRT-PCR assay. Effects of miR-135b inhibition on IL-6 and IL-8 expression, as determined in panel A. (C) Effects of miR-135b inhibition on IL-17F production were analyzed in Karpas 299 cells by ELISA. (D) Effects of miR-135b inhibition on granzyme B (GZMB) and perforin 1 (PRF1) expression, as determined in panel A. miR-135b blockade did not affect the expression levels of IL-21, IL-23, and TGF-β1 (data not shown; $^{*}P < .05$; $^{**}P < .01$; $^{***}P < .001$).

expression of Th17-cell–associated molecules (IL-17A, IL-17F, and retinoic acid-related orphan receptor [ROR]γ), overlapping with Th17 cells phenotype, low expression of GATA3, and suppression of TCR components, as summarized in Figure 4B.[15] Previous studies also have demonstrated that both Th1 and Th2 differentiation programs antagonize Th17-cell differentiation.[24]

Along with these observations, reassessment of computational prediction proposed that miR-135b potentially targets 2 Th2 master regulators GATA3 and STAT6 (Figure 4C and supplemental Figure 3B). The GSEA result also supported the possibility of STAT6 as a miR-135b target (supplemental Figure 3A). We thus investigated the immune modulatory property of miR-135b on ALCL immunophenotype overlapping with Th17 cells. Luciferase assays revealed that miR-135b targets the 3′UTRs of both STAT6 and GATA3 (Figure 4D). Mutagenesis of potential target sites in their 3′UTR abrogated the response of STAT6 and GATA3 3′UTR to miR-135b, confirming direct interactions of miR-135b with STAT6 and GATA3 (Figure 4D). We further found that suppression of miR-135b indeed up-regulates protein expression of STAT6 and GATA3 in ALCL cells, demonstrating that both STAT6 and GATA3 are intrinsic targets of miR-135b in ALCL cells (Figure 4E and supplemental Figure 3C).

miR-135b blockade suppresses IL-17 production by ALCL cells

IL-4–STAT6 axis and GATA3 are important for Th2 differentiation of normal lymphocytes.[25] In normal lymphocyte differentiation, lineage-specific transcription factors can both activate and repress differentiation programs.[26,27] GATA3 simultaneously promotes Th2 differentiation and represses Th1 differentiation, because Th1 regulator T-bet has opposing bidirectional effects.[25] A similar relationship also exists between Th1 and Th2 differentiaton programs and Th17 differentiation programs. As Th1 and Th2 effector cytokines (IFN-γ and IL-4) antagonize Th17 differentiation,[24] both GATA3 and T-bet have been shown to suppress Th17 differentiation.[27,28] On the basis of these concepts, we next examined the effects of miR-135b suppression on the expressions of Th17-related molecules. Karpas 299 ALCL cells endogenously expressed IL-17, and miR-135b suppression attenuated the expression levels of IL-17A and IL-17F transcripts (Figure 5A), consistent with GATA3-mediated suppression of Th17 differentiation.[28] Blockade of miR-135b also suppressed the expression of IκBζ, a recently identified key regulator of Th17 differentiation,[29] without concomitant changes of RORγ, RORα, or aryl hydrocarbon receptor. In addition, down-regulation of proinflammatory cytokines including IL-6 and IL-8 was observed by miR-135b suppression (Figure 5B). Consistently, we confirmed that miR-135b suppression attenuates IL-17 production in Karpas 299 cells (Figure 5C). Taken together, these findings suggest that NPM-ALK/STAT3–miR-135b axis polarizes the identity of ALCL cells to the IL-17–producing immunophenotype resembling Th17 cells by suppression of GATA3 and STAT6. In addition, miR-135b knockdown suppressed the expression of granzyme B and perforin 1, cytotoxic molecules highly expressed in ALCL (Figure 5D),[15] suggesting that miR-135b affects the broad range of ALCL immunophenotype.

Modulation of paracrine inflammatory reaction and tumorigenic potential of ALCL by miR-135b

IL-17 is a proinflammatory cytokine that stimulates the production of various inflammatory cytokines (eg, IL-1β, IL-6, IL-8, G-CSF,

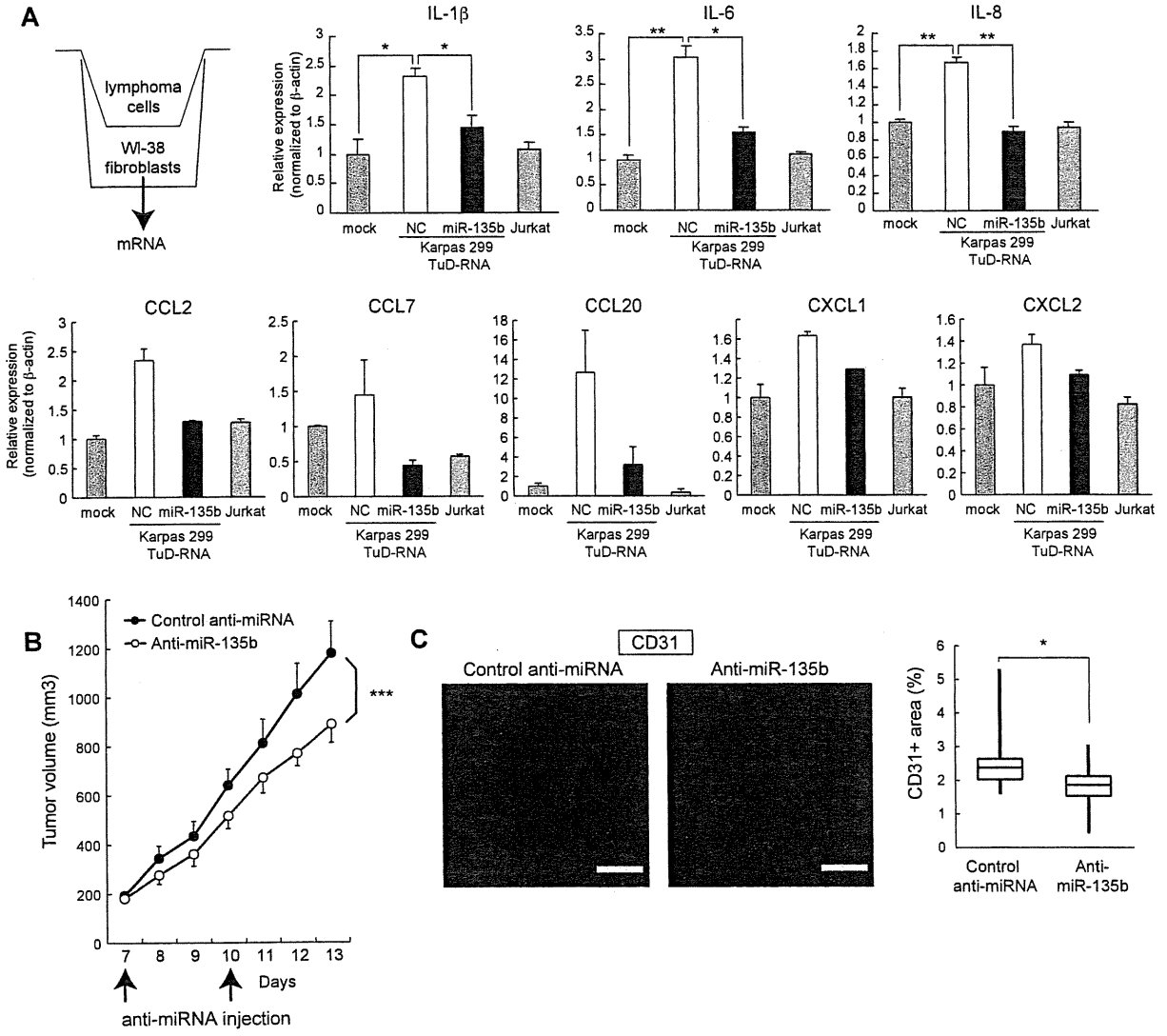

Figure 6. Regulation of paracrine inflammatory reaction and tumorigenic potential by miR-135b. (A) ALCL cells stimulate proinflammatory cytokine (IL-1β, IL-6, and IL-8) and chemokine (CCL2, CCL7, CCL20, CXCL1, and CXCL2) production in human fibroblasts through an miR-135b–dependent manner. WI-38 human fibroblasts were cocultured with Karpas 299 or Jurkat cells and subjected to qRT-PCR assay (*$P < .05$; **$P < .01$). (B) Growth curves of Karpas 299 subcutaneous tumors after transplantation into SCID mice and administration with miR-135 antisense–atelocollagen or control oligonucleotide–atelocollagen complexes. After random assignment at day 7 after inoculation (n = 6/group), LNA-based antisense oligonucleotides (5μM) with atelocollagen were administered into the subcutaneous spaces around the tumors at days 7 and 10 and measured (means ± SEM; ***$P < .001$). (C) Effects of miR-135b inhibition on tumor angiogenesis. Representative images of CD31 immunostaining of tumor sections (left) and quantification of microvessel density measured by CD31-positive area (right). Pixel density was quantified in multiple tumor images from 6 mice per group using ImageJ 1.36b software. Scale bar represents 100 μm (*$P < .05$).

and GM-CSF) and chemokines (eg, CCL2, CCL7, CCL20, CXCL1, and CXCL2) from many cell types, such as fibroblasts, endothelial cells, and neutrophils, and is involved in pathogenesis of autoimmune disorders.[30] Although the significance of IL-17 in cancer is largely unknown and might depend on cancer-type and context, proinflammatory and proangiogenic properties of IL-17 have been associated with tumor progression in several studies.[31-34] In this setting, IL-17 has been shown to augment the secretion of angiogenic chemokines, such as CXCL1 and CXCL5.[34] We analyzed the operational role of miR-135b in tumor development of ALCL. Accordingly, coculture experiments demonstrated that Karpas 299 cells stimulate the production of proinflammatory cytokines (IL-1β, IL-6, and IL-8) and chemokines (CCL2, CCL7, CCL20, and CXCL1/2) in WI-38 human fibroblasts in an miR-135b–dependent manner (Figure 6A), underscoring the involvement of miR-135b in paracrine inflammatory response.

We also examined the roles of miR-135b in ALCL tumorigenic potential in vivo. In a xenograft model, local administration of LNA-based miRNA inhibitors against miR-135b with atelocollagen suppressed the growth of subcutaneous Karpas 299 tumors (Figure 6B). Furthermore, the inhibition of in vivo tumor growth by anti–miR-135b antisense was accompanied with reduced tumor angiogenesis (Figure 6C). These results thus collectively suggest that miR-135b–mediated modulation of paracrine inflammatory reaction favors tumor microenvironment, also indicating a therapeutic significance of targeting this axis by miR-135b interference.

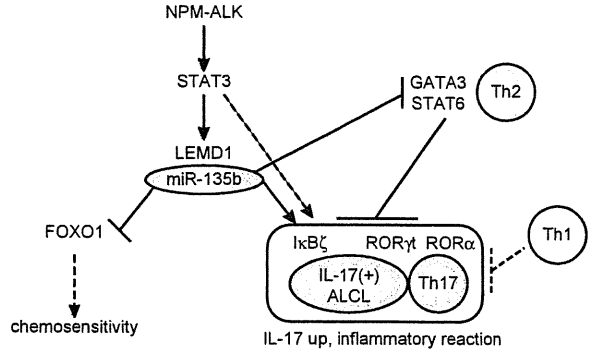

Figure 7. Summary of roles of miR-135b in ALCL pathogenesis. The present study demonstrates that NPM-ALK induces LEMD1 and miR-135b expression through STAT3 in ALCL and that miR-135b targets FOXO1 and two versatile Th2 regulators, GATA3, and STAT6, rendering the IL-17–producing immunophenotype to ALCL.

Discussion

Here, we identified miR-135b as a downstream mediator of NPM-ALK/STAT3 signaling (Figure 7). Although NPM-ALK drives malignant transformation of ALCL cells through various downstream signaling pathways, including STAT3, Ras-ERK, and PI3K,[9] our study demonstrated the oncogenic aspect of miR-135b targeting FOXO1 in ALCL pathogenesis (Figure 7). It was shown previously that miR-135b is highly expressed in embryonic stem cells and other cancer types, including colorectal and prostate cancer.[19,35,36] Considering the essential roles in embryonic stem cells and the pivotal oncogenic functions of STAT3,[37] the STAT3–miR-135b pathway might be widely used in these conditions. Oncogenic roles of miR-135b also might be supported by up-regulation of its host LEMD1, which is alternatively known as cancer/testis antigen 50, and DNA copy number gain in 1q32.1 in colorectal tumors.[38-40] Although the biologic function(s) of LEMD1 has not been investigated so far, LEMD1 also might contribute to NPM-ALK–driven oncogenicity and IL-17–producing immunophenotype in ALCL. Considering other reports linking NPM-ALK to inhibition of FOXO3a activity through PI3K/Akt pathway,[21] NPM-ALK might engage multiple players, including noncoding RNAs to prevent these central tumor suppressor pathways from activating by NPM-ALK–induced oncogenic stresses. We also examined miR-135b expression levels in lung cancer and neuroblastoma cell lines carrying ALK abnormalities (supplemental Table 4 and Figure 4). miR-135b expression was very low in neuroblastoma cell lines examined. The H2228 lung adenocarcinoma cell line containing EML4-ALK fusion expressed miR-135b to some extent, although at a lower level than ALCL cells. Involvement of miR-135b in the pathogenesis of some other tumor subtypes engaging ALK abnormalities remains to be further elucidated.

Importantly, we uncovered an interesting immune modulatory property of miR-135b. miR-135b targeted Th2 master regulators STAT6 and GATA3, and inhibition of miR-135b suppressed IL-17 production by ALCL cells, evidencing the Th17-skewing effect of miR-135b. ALK-positive ALCL is characterized by the presence of NPM-ALK and was originally described as a T- or null-cell phenotype. Loss of T-cell phenotype frequently observed in ALCL, shown by decreased expression of αβ-TCR heterodimer and CD3ε, has been demonstrated to be partly mediated by the perturbation by NPM-ALK signaling.[23] Conversely, it is postulated that the normal counterpart of ALCL is an activated mature cytotoxic T-cell, because of the expression of cytotoxic granule-associated molecules such as TIA1, gramzyme B, and perforin 1, although CD8 is usually negative in ALCL and CD4 is positive in 70% cases of ALCL.[41] In addition to this aberrant phenotype, a recent molecular signature study of PTCL revealed that ALCL displays up-regulation of Th17-cell–associated molecules (IL-17A, IL-17F, and RORγ) and down-regulation of GATA3. The immunophenotype overlaps with that of Th17 cells, compared with other lymphoma subtypes such as angioimmunoblastic T-cell lymphoma (AITL), ALK-negative ALCL, adult T-cell leukemia/lymphoma, and PTCL-unclassifiable.[15] In support of this notion, a most recent report demonstrates that levels of IL-17, IL-8, and IL-22 were elevated in untreated ALK-positive ALCL patients' sera but undetectable in those of complete remission after chemotherapy,[42] reinforcing the relevance of IL-17–producing immunophenotype of ALCL. Although the underlying mechanisms determining the immunophenotypes of various lymphomas have been largely unresolved, our study has demonstrated that a signaling network elicited by ectopic expression of NPM-ALK oncogene and its downstream miRNA confers the aberrant immunophenotype of ALCL cells.

Importance of tumor microenvironment in lymphoma development has been well investigated in B-cell lymphoma, including Hodgkin lymphoma.[43] A recent report has shown that IL-17–positive cells were more frequently observed in AITL than in PTCL-unclassifiable and that both Th17 and mast cells contribute to the lymphoma-associated proinflammatory environment in AITL.[44] In contrast, ALCL is unique in the respect that ALCL cells produce IL-17 by themselves, which might result in different clinical features between these lymphoma subtypes. In consistent with strong effects of IL-17 on neutrophils, extensive neutrophil infiltration has been observed in some cases of ALCL, as referred to as neutrophil-rich ALCL, which can sometimes be misdiagnosed as an inflammatory disease rather than lymphoma.[45-47] Frequent B symptoms in ALCL also might be attributable to this IL-17–producing immunophenotype. In this study, antisense-based miR-135b blockade reduced tumor angiogenesis and growth in an in vivo tumor model, which observation is consistent with the proangiogenic function of IL-17 (Figure 6).[33,34] Although a line of observations suggest both pro- and antitumor potentials of IL-17 or Th17 cells in a context-dependent manner,[31,32] the tumor-suppressive effect of miR-135b inhibition suggests that local proinflammatory properties of IL-17–producing ALCL cells may provide the favorable tumor microenvironment through the enhancement of angiogenesis or so in this context. Recent evidence has revealed that many characteristic aspects of cancer-related biologic processes, including drug resistance, maintenance of cancer-initiating cells, and metastasis, are associated with miRNA function.[48] The present study demonstrates another unique contribution of miRNA dysregulation to tumor development, ie, modulation of immunophenotype of lymphoma cells and the consequent alteration of tumor milieu by miR-135b.

Among hundreds of miRNAs, miR-326 has been identified so far as a regulator of Th17 differentiation, which promoted Th17 differentiation via targeting ETS1.[49] In addition, miR-155 was recently shown to promote Th17 cell formation in a $CD4^+$ T-cell intrinsic manner.[50] It was consistent with the finding that miR-155 targets Th2 promoter c-Maf. Our study suggests the presence of additional regulatory miRNAs of Th17 differentiation through the inhibition of differentiation program(s) to other helper T-cell lineage(s). Generally, lineage-specific transcription factors and cytokines can interfere with the differentiation to other helper T-cell subsets. Although it requires careful assessment about

difference between normal lymphocyte differentiation and lymphoma cell phenotype polarization, our findings suggest that miRNAs might be widely involved in this reciprocal regulatory network between helper T-cell differentiation programs. The STAT3–miR-135b–GATA3/STAT6 connection revealed in this study might propose inhibitory mechanism(s) against Th2 in Th17 differentiation program, mirroring the opposite inhibitory impacts of Th1 and Th2 programs on Th17 differentiation,[24,26] for ensuring mutual exclusion.

In conclusion, our study demonstrates a novel oncogenic pathway composed of NPM-ALK, STAT3, and miR-135b that authorizes IL-17–producing immunophenotype of ALCL. Tumor suppression with miR-135b blockade also demonstrates the therapeutic potential of miR-135b interference strategy targeting the "Th17 mimic" axis. These findings might advance our understandings of ALK-mediated oncogenesis and be useful for the development of new therapeutic interventions.

Acknowledgments

The authors thank E. Johansson, Y. Morishita, K. Kiyono, M. Morikawa, Y. Yoshimatsu, K. Isogaya, and H. Mihira for discussion and skilled technical assistance and all members of the Department of Molecular Pathology, University of Tokyo.

This work was supported by KAKENHI (Grants-in-Aid for Scientific Research for Research Activity start-up 22890038 and Innovative Areas "RNA regulation" 23112702); the Global Center of Excellence Program for "Integrative Life Science Based on the Study of Biosignaling Mechanisms" from the Ministry of Education, Culture, Sports, Science and Technology of Japan; and the Cell Science Research Foundation.

Authorship

Contribution: H. Matsuyama and H.I.S. conceived and designed the research; H. Matsuyama performed experiments and analyses and wrote the paper; H.I.S. provided key materials and analyzed and wrote the paper; H.N. performed animal experiments and analysis; M.N., T.Y., N.K., H. Mano and K.S. provided clinical samples; and K.S. and K.M. supervised the whole project and wrote the paper.

Conflict-of-interest disclosure: The authors declare no competing financial interests.

Correspondence: Kohei Miyazono, Department of Molecular Pathology, Graduate School of Medicine, University of Tokyo, 7-3-1 Hongo, Bunkyo-ku, Tokyo 113-0033, Japan; e-mail: miyazono@m.u-tokyo.ac.jp.

References

1. Ambros V, Chen X. The regulation of genes and genomes by small RNAs. *Development.* 2007; 134(9):1635-1641.
2. O'Connell RM, Rao DS, Chaudhuri AA, Baltimore D. Physiological and pathological roles for microRNAs in the immune system. *Nat Rev Immunol.* 2010; 10(2):111-122.
3. Croce CM. Causes and consequences of microRNA dysregulation in cancer. *Nat Rev Genet.* 2009;10(10):704-714.
4. Staudt LM, Dave S. The biology of human lymphoid malignancies revealed by gene expression profiling. *Adv Immunol.* 2005;87:163-208.
5. Alizadeh AA, Eisen MB, Davis RE, et al. Distinct types of diffuse large B-cell lymphoma identified by gene expression profiling. *Nature.* 2000; 403(6769):503-511.
6. Suzuki HI, Miyazono K. Emerging complexity of microRNA generation cascades. *J Biochem.* 2011;149(1):15-25.
7. He L, Thomson JM, Hemann MT, et al. A microRNA polycistron as a potential human oncogene. *Nature.* 2005;435(7043):828-833.
8. Suzuki HI, Yamagata K, Sugimoto K, Iwamoto T, Kato S, Miyazono K. Modulation of microRNA processing by p53. *Nature.* 2009;460(7254):529-533.
9. Chiarle R, Voena C, Ambrogio C, Piva R, Inghirami G. The anaplastic lymphoma kinase in the pathogenesis of cancer. *Nat Rev Cancer.* 2008;8(1):11-23.
10. Soda M, Choi YL, Enomoto M, et al. Identification of the transforming EML4-ALK fusion gene in non-small-cell lung cancer. *Nature.* 2007; 448(7153):561-566.
11. Haraguchi T, Ozaki Y, Iba H. Vectors expressing efficient RNA decoys achieve the long-term suppression of specific microRNA activity in mammalian cells. *Nucleic Acids Res.* 2009;37(6):e43.
12. Piva R, Pellegrino E, Mattioli M, et al. Functional validation of the anaplastic lymphoma kinase signature identifies CEBPB and BCL2A1 as critical target genes. *J Clin Invest.* 2006;116(12):3171-3182.
13. Anastasov N, Klier M, Koch I, et al. Efficient shRNA delivery into B and T lymphoma cells using lentiviral vector-mediated transfer. *J Hematop.* 2009;2(1):9-19.
14. Bromberg JF, Wrzeszczynska MH, Devgan G, et al. Stat3 as an oncogene. *Cell.* 1999;98(3): 295-303.
15. Iqbal J, Weisenburger DD, Greiner TC, et al. Molecular signatures to improve diagnosis in peripheral T-cell lymphoma and prognostication in angioimmunoblastic T-cell lymphoma. *Blood.* 2010; 115(5):1026-1036.
16. Subramanian A, Tamayo P, Mootha VK, et al. Gene set enrichment analysis: a knowledge-based approach for interpreting genome-wide expression profiles. *Proc Natl Acad Sci U S A.* 2005;102(43):15545-15550.
17. Lawrie CH, Saunders NJ, Soneji S, et al. MicroRNA expression in lymphocyte development and malignancy. *Leukemia.* 2008;22(7): 1440-1446.
18. Saito T, Saetrom P. MicroRNAs–targeting and target prediction. *N Biotechnol.* 2010; 27(3):243-249.
19. Nagel R, le Sage C, Diosdado B, et al. Regulation of the adenomatous polyposis coli gene by the miR-135 family in colorectal cancer. *Cancer Res.* 2008;68(14):5795-5802.
20. Kuiper RP, Schoenmakers EF, van Reijmersdal SV, et al. High-resolution genomic profiling of childhood ALL reveals novel recurrent genetic lesions affecting pathways involved in lymphocyte differentiation and cell cycle progression. *Leukemia.* 2007;21(6):1258-1266.
21. Gu TL, Tothova Z, Scheijen B, Griffin JD, Gilliland DG, Sternberg DW. NPM-ALK fusion kinase of anaplastic large-cell lymphoma regulates survival and proliferative signaling through modulation of FOXO3a. *Blood.* 2004;103(12): 4622-4629.
22. Greer EL, Brunet A. FOXO transcription factors at the interface between longevity and tumor suppression. *Oncogene.* 2005;24(50):7410-7425.
23. Ambrogio C, Martinengo C, Voena C, et al. NPM-ALK oncogenic tyrosine kinase controls T-cell identity by transcriptional regulation and epigenetic silencing in lymphoma cells. *Cancer Res.* 2009;69(22):8611-8619.
24. Harrington LE, Hatton RD, Mangan PR, et al. Interleukin 17-producing CD4+ effector T cells develop via a lineage distinct from the T helper type 1 and 2 lineages. *Nat Immunol.* 2005;6(11):1123-1132.
25. Zhou M, Ouyang W. The function role of GATA-3 in Th1 and Th2 differentiation. *Immunol Res.* 2003;28(1):25-37.
26. McGeachy MJ, Cua DJ. Th17 cell differentiation: the long and winding road. *Immunity.* 2008;28(4): 445-453.
27. Lazarevic V, Chen X, Shim JH, et al. T-bet represses T(H)17 differentiation by preventing Runx1-mediated activation of the gene encoding RORgammat. *Nat Immunol.* 2011;12(1):96-104.
28. van Hamburg JP, Mus AM, de Bruijn MJ, et al. GATA-3 protects against severe joint inflammation and bone erosion and reduces differentiation of Th17 cells during experimental arthritis. *Arthritis Rheum.* 2009;60(3):750-759.
29. Okamoto K, Iwai Y, Oh-Hora M, et al. IkappaBzeta regulates T(H)17 development by cooperating with ROR nuclear receptors. *Nature.* 2010; 464(7293):1381-1385.
30. Yang XO, Chang SH, Park H, et al. Regulation of inflammatory responses by IL-17F. *J Exp Med.* 2008;205(5):1063-1075.
31. Ji Y, Zhang W. Th17 cells: positive or negative role in tumor? *Cancer Immunol Immunother.* 2010;59(7):979-987.
32. Zou W, Restifo NP. T(H)17 cells in tumour immunity and immunotherapy. *Nat Rev Immunol.* 2010; 10(4):248-256.
33. Numasaki M, Fukushi J, Ono M, et al. Interleukin-17 promotes angiogenesis and tumor growth. *Blood.* 2003;101(7):2620-2627.
34. Numasaki M, Watanabe M, Suzuki T, et al. IL-17 enhances the net angiogenic activity and in vivo growth of human non-small cell lung cancer in SCID mice through promoting CXCR-2-dependent angiogenesis. *J Immunol.* 2005;175(9): 6177-6189.

35. Lin CH, Jackson AL, Guo J, Linsley PS, Eisenman RN. Myc-regulated microRNAs attenuate embryonic stem cell differentiation. *EMBO J.* 2009;28(20):3157-3170.
36. Tong AW, Fulgham P, Jay C, et al. MicroRNA profile analysis of human prostate cancers. *Cancer Gene Ther.* 2009;16(3):206-216.
37. Bowman T, Garcia R, Turkson J, Jove R. STATs in oncogenesis. *Oncogene.* 2000;19(21):2474-2488.
38. Yuki D, Lin YM, Fujii Y, Nakamura Y, Furukawa Y. Isolation of LEM domain-containing 1, a novel testis-specific gene expressed in colorectal cancers. *Oncol Rep.* 2004;12(2):275-280.
39. Jones AM, Douglas EJ, Halford SE, et al. Array-CGH analysis of microsatellite-stable, near-diploid bowel cancers and comparison with other types of colorectal carcinoma. *Oncogene.* 2005;24(1):118-129.
40. Douglas EJ, Fiegler H, Rowan A, et al. Array comparative genomic hybridization analysis of colorectal cancer cell lines and primary carcinomas. *Cancer Res.* 2004;64(14):4817-4825.
41. Swerdlow SH, Campo E, Harris NL, et al. *WHO Classification of Tumours of Haematopoietic and Lymphoid Tissues.* 4th ed. Lyon, France: IARC; 2008.
42. Savan R, McFarland AP, Reynolds DA, et al. A novel role for IL-22R1 as a driver of inflammation. *Blood.* 2011;117(2):575-584.
43. Küppers R. The biology of Hodgkin's lymphoma. *Nat Rev Cancer.* 2009;9(1):15-27.
44. Tripodo C, Gri G, Piccaluga PP, et al. Mast cells and Th17 cells contribute to the lymphoma-associated pro-inflammatory microenvironment of angioimmunoblastic T-cell lymphoma. *Am J Pathol.* 2010;177(2):792-802.
45. Mann KP, Hall B, Kamino H, Borowitz MJ, Ratech H. Neutrophil-rich, Ki-1-positive anaplastic large-cell malignant lymphoma. *Am J Surg Pathol.* 1995;19(4):407-416.
46. Tamiolakis D, Georgiou G, Prassopoulos P, Simopoulos C, Venizelos J, Papadopoulos N. Neutrophil-rich anaplastic large cell lymphoma (NR-ALCL) mimicking lymphadenitis: a study by fine-needle aspiration biopsy. *Leuk Lymphoma.* 2004;45(6):1309-1310.
47. Engsig FN, Moller MB, Hasselbalch HK, Mahdi B, Obel N. Extreme neutrophil granulocytosis in a patient with anaplastic large cell lymphoma of T-cell lineage. *APMIS.* 2007;115(6):778-783.
48. Suzuki HI, Miyazono K. Dynamics of microRNA biogenesis: crosstalk between p53 network and microRNA processing pathway. *J Mol Med.* 2010;88(11):1085-1094.
49. Du C, Liu C, Kang J, et al. MicroRNA miR-326 regulates TH-17 differentiation and is associated with the pathogenesis of multiple sclerosis. *Nat Immunol.* 2009;10(12):1252-1259.
50. O'Connell RM, Kahn D, Gibson WS, et al. MicroRNA-155 promotes autoimmune inflammation by enhancing inflammatory T cell development. *Immunity.* 2010;33(4):607-619.

Dicer Plays Essential Roles for Retinal Development by Regulation of Survival and Differentiation

Atsumi Iida,[1,2] *Toru Shinoe,*[1,2] *Yukihiro Baba,*[1] *Hiroyuki Mano,*[3] *and Sumiko Watanabe*[1]

Purpose. Much attention has been paid to the roles of microRNA in developmental and biological processes. Dicer plays essential roles in cell survival and proliferation in various organs. We examined the role of Dicer in retinal development using retina-specific conditional knockout of Dicer in mice.

Methods. Dkk3-Cre expressed the *Cre* gene in retinal progenitor cells from an early embryonic stage. The authors analyzed Dkk-Cre/Dicer-flox (Dicer-CKO) mice for their survival, proliferation, and differentiation. To analyze the role of Dicer in later stages of retinal development, a Cre expression plasmid was introduced into the neonatal retina by electroporation, and retinal differentiation was examined.

Results. Dicer-CKO mice were born at the numbers we expected, based on Mendelian genetics, but their eyes never opened. Massive death of retinal progenitor cells occurred during embryogenesis, resulting in microphthalmia, and most retinal cells had disappeared by postnatal day 14. In vitro reaggregation culture of Dicer-CKO retinal cells showed that cell death and the suppression of proliferation by Dicer inactivation occurred in a cell-autonomous manner. Cell differentiation markers were expressed in the Dicer-CKO retina; however, these cells localized abnormally, and the inner plexiform layer was absent, suggesting that cell migration and morphologic differentiation, especially process extension, were perturbed. Forced neonatal expression of Cre induced apoptosis and affected the expression of differentiation markers.

Conclusions. Taken together, these results show that Dicer is essential during early retinal development. (*Invest Ophthalmol Vis Sci.* 2011;52:3008-3017) DOI:10.1167/iovs.10-6428

The vertebrate neural retina is organized into a laminar structure comprising six types of neuron and glial cell, including Müller glia and microglia. During retinogenesis, these various cell types are derived from a common population of multipotent retinal progenitor cells in a relatively fixed chronological sequence.[1] Intrinsic cues and extrinsic signals play critical roles in defining the types of cells generated from common retinal progenitor cells,[2,3] and various molecules are involved in this process. The expression of these genes in retinal development is regulated at various levels; microRNA (miRNA) is one such regulator.

MicroRNAs are small, noncoding RNAs that are encoded in the genomes of all metazoans. They are essential in the proliferation and differentiation of various tissues, including stem cells.[4-6] The roles of miRNAs in retina have been reported,[7,8] and a recent study showed the presence of light-regulated retinal miRNAs.[9] In addition to suppressing the function of certain miRNAs, we can remove all miRNAs by deleting enzymes that are essential in their biosynthesis. DGCR8 is required for the production of all canonical miRNAs, and Dicer is an enzyme that cleaves double-stranded RNA into miRNA.[10] The removal of DGCR8 or Dicer results in a defective cell cycle and silencing of the self-renewal program of embryonic stem cells.[11,12] Because the complete loss of Dicer in mice results in early embryonic death,[13] mice with a conditional allele of the Dicer gene have been produced,[14] enabling the study of the roles of miRNA in organogenesis. Subsequently, essential roles of Dicer in organogenesis have been revealed by studying mice with various tissue-specific expression of Cre.[14,15]

In neurons, the deletion of Dicer by α-calmodulin kinase II Cre results in an array of phenotypes, including microcephaly and reduced dendritic branch elaboration, suggesting that the loss of Dicer disrupts cellular and tissue morphogenesis in the cortex and hippocampus.[16] The first study examining the roles of Dicer in the retina using Chx10-Cre transgenes, expected to express Cre in retinal progenitor cells, showed that although Chx10 was expressed in the embryonic retina, morphologic defects were observed at postnatal day (P) 16 with the formation of photoreceptor rosettes, accompanied by abnormal electroretinogram responses.[17] However, the relatively mild phenotype of the mice is surmised to be caused by mosaic expression of Cre in the Chx10-Cre transgenic retina[17] because subsequent work by George and Reh using αPax6-Cre-retina specific Dicer conditional knockout showed that Dicer is required in retinal development.[18] In this work, we evaluated the effects of deleting Dicer using Dkk3-Cre mice, which expressed the *Cre* gene in retinal progenitor cells from an early embryonic stage.[19]

Materials and Methods

Mice and Reagents

EGFP transgenic mice, which express the *EGFP* gene ubiquitously through the CAG promoter, were kindly provided by Masaru Okabe (Osaka University).[20,21] $Dicer^{flox}$ mice[14] were kindly provided by Michael McManus (University of California, San Francisco), and Dkk3-Cre BAC transgenic mice were as previously described.[19] $Dicer^{flox/flox}$ (Dicer-fl/fl) or $Dicer^{flox/wild}$ were used as controls for experiments shown in Figures 1 and 2. ICR mice were obtained from Japan SLC Co. All animal experiments were approved by the Animal Care Committee of the Institute of Medical Science, University of Tokyo, and were conducted in accordance with the ARVO Statement for the Use of Animals in Ophthalmic and Vision Research.

From the [1]Division of Molecular and Developmental Biology, Institute of Medical Science, University of Tokyo, Tokyo, Japan; and the [3]Division of Functional Genomics, Jichi Medical University, Tochigi, Japan.

[2]These authors contributed equally to the work presented here and should therefore be regarded as equivalent authors.

Supported by MEXT, Japan.

Submitted for publication August 18, 2010; revised October 18 and December 7 and 14, 2010; accepted December 15, 2010.

Disclosure: **A. Iida**, None; **T. Shinoe**, None; **Y. Baba**, None; **H. Mano**, None; **S. Watanabe**, None

Corresponding author: Sumiko Watanabe, Division of Molecular and Developmental Biology, Institute of Medical Science, University of Tokyo, 4-6-1 Shirokanedai, Minato-ku, Tokyo 108-8639, Japan; sumiko@ims.u-tokyo.ac.jp.

Investigative Ophthalmology & Visual Science, May 2011, Vol. 52, No. 6

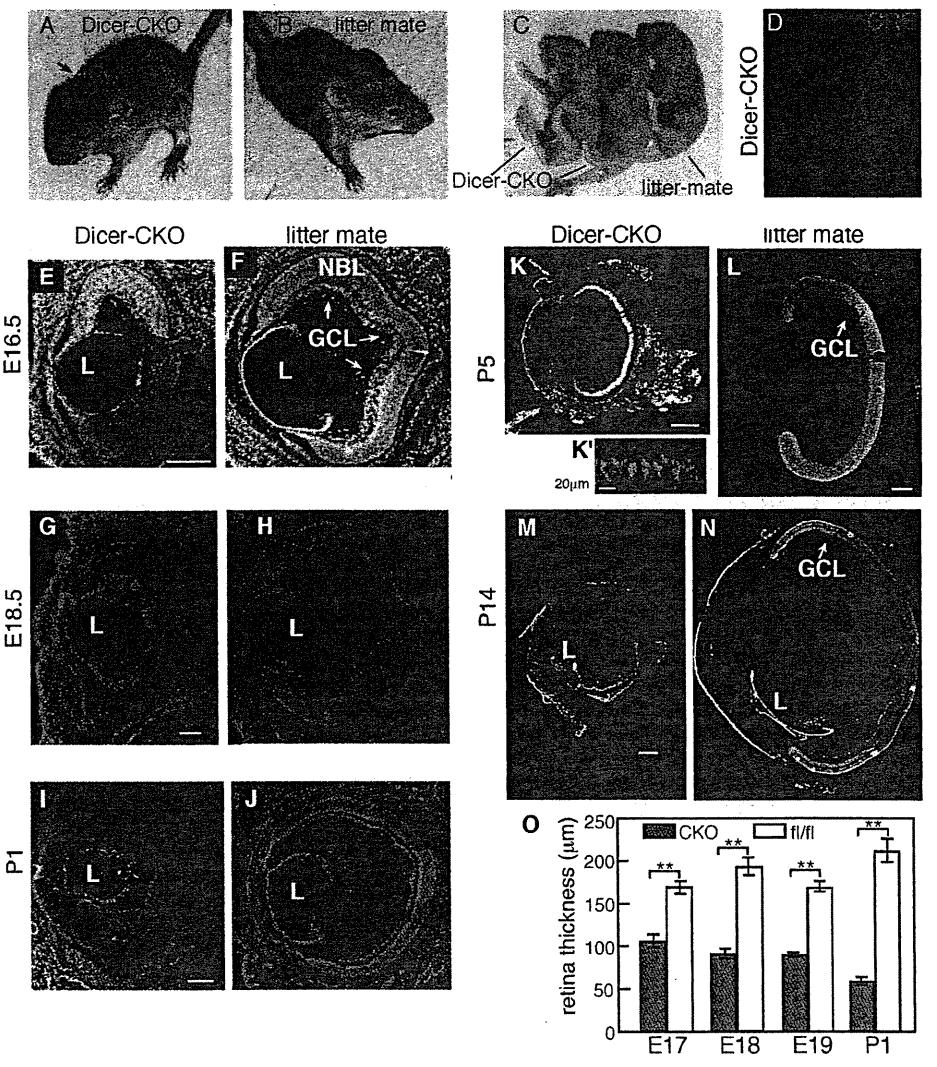

FIGURE 1. Dicer$^{lox/lox}$:Dkk3$^{+/cre}$ (Dicer-CKO) mice were born but had microphthalmia. (**A–C**) Images of Dicer-CKO (**A**) and littermate (**B**) mice at 2 weeks of age. Images of embryos of Dicer-CKO and littermate at E16.5 (**C**). (**D**) Immunostaining of Cre expression of Dicer-CKO retina at E17.5 was performed using frozen sections. (**E–N**) Structure of the eye of Dicer-CKO and littermate at E16.5 (**E**, **F**), E18.5 (**G**, **H**), P1 (**I**, **J**), P5 (**K**, **L**), and P14 (**M**, **N**) stages. Head (**E–J**) or whole eyes (**K–N**) were frozen sectioned, and nuclei were visualized by staining of DAPI. L, lens. Scale bar, 200 μm unless indicated. L, lens; NBL, neuroblastic layer. (**O**) Thickness of retina of Dicer-CKO or fl/fl control mice. Measurements were made under a microscope, and the thickness of retina at central region was examined at indicated stages. Average of three independent retinas with SD is shown. $^{**}P < 0.01$, Student's *t*-test.

DNA Construction

pxCANCre containing CAG promoter followed by *Cre* genes was the gift of Izumu Saito (University of Tokyo). CAG-Cre-IRES-EGFP was constructed by the ligation of fragments of CAG-Cre (*SalI-BglII*), IRES-EGFP (*BglII-NotI*), and the vector portion from pEGFP2 (*SalI-NotI*).

Immunostaining

Immunostaining of sectioned or dissociated retina was performed as described previously.[22] OCT compound (Tissue-Tek)–embedded samples were sectioned with 10-μm thickness by a cryostat (CM3050S; Leica, Wetzlar, Germany). Primary antibodies used were the following: mouse monoclonal antibodies against βIII tubulin (Covance, Princeton, NJ), photoreceptor-specific nuclear receptor ([PNR], ppmx), rhodopsin (Rho4D2, kindly donated by Robert S. Molday, University of British Columbia), glutamine synthetase (GS; Chemicon, Temecula, CA), HuC/D (Molecular Probes, Eugene, OR), Ki67 (BD Biosciences, Franklin Lakes, NJ), Cre (Millipore, Billerica, MA), rabbit polyclonal antibody against GFP (Clontech, Palo Alto, CA), Pax6 (Covance), calbindin (Millipore), active-caspase3 (Promega, Madison, WI), and goat polyclonal antibody anti-Brn3b (Santa Cruz Biotechnology, Santa Cruz, CA). All antibodies against retinal subtypes have been used by us and confirmed to recognize mouse retina.[23–25] The first antibodies were visualized by using appropriate Alexa 488 or Alexa 546-conjugated secondary antibodies (Molecular Probes). Samples were mounted in reagent (VectaShield; Vector Laboratories, Burlingame, CA) and analyzed under a microscope (Axioplan; Zeiss, Oberkochen, Germany).

Retinal Cultures and Electroporation

Reaggregation cultures were set up as described earlier.[23] Briefly, retinal cells of Dicer-CKO:GFP or GFP mice at embryonic day (E) 16 were dissociated and mixed with far larger numbers of host retinal cells isolated from normal ICR mice at E16. The ratio of donor to host cells was 5:95. Electroporation was performed using an electroporator (CUY21; Nepa Gene, Chiba, Japan) and electrode (CYU520P5; Nepa Gene), as described.[26] Briefly, retinas were transferred to a microelectroporation chamber filled with plasmid solution (1 mg/mL in Hanks' balanced salt solution), and four square pulses (25 V) of 50-μs duration with 950-μs intervals were applied using a pulse generator (CUY21; Nepa Gene).

RESULTS

Inactivation of Dicer in Retinal Progenitor Cells Results in Severe Retinal Malformation

To inactivate Dicer in retinal progenitor cells, we used Dkk3-Cre mice, which express Cre recombinase beginning on at least E10.5 in a retina-specific manner.[19] The expected num-

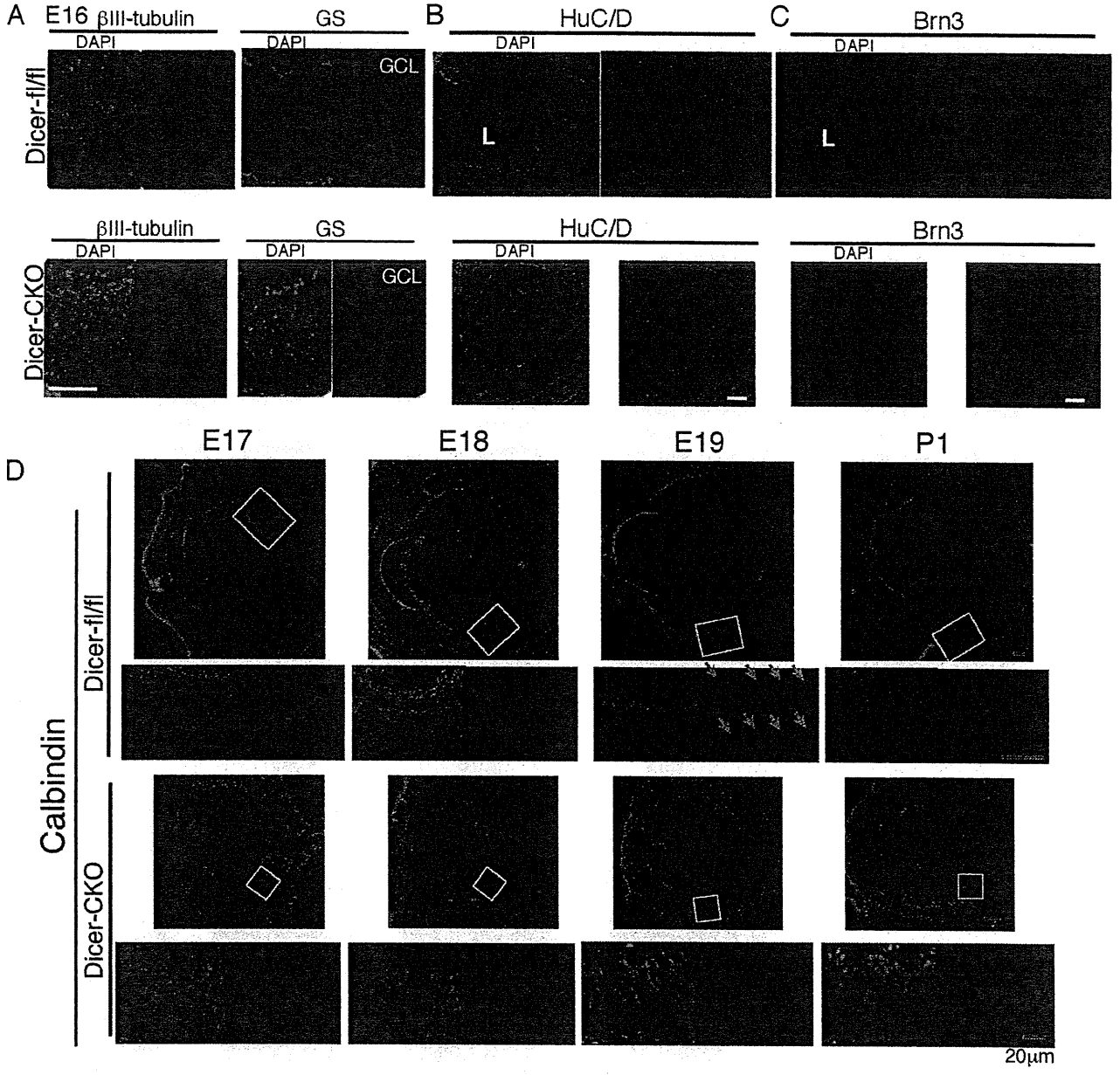

FIGURE 2. Detailed examination of retinal development by immunostaining of retinas of Dicer-CKO mice revealed perturbation of retinal development. (**A–D**) Retinas from Dicer-CKO or littermate control mice at E16 (**A–C**) or indicated stages (**D**) were frozen sectioned. Immunostaining using indicated antibodies was performed, and nuclei were visualized by staining of DAPI. (**D**) *Lower* panels are enlarged images of the *white squared regions* in the *upper* panels. L, lens. Scale bars: 100 μm (**A**, **D**); 200 μm (**B**, **C**).

bers of $Dicer^{flox/flox}/Dkk3^{cre/-}$ (Dicer-CKO) mice, based on Mendelian genetics, were born, but they died approximately 4 to 6 weeks after birth for unknown reasons. Their eyes never opened (Fig. 1A), and they had small earlobes (Fig. 1A, red arrows), probably because of undetectable expression of Dkk3 in this region. The Dicer-CKO embryos were indistinguishable from their littermates in their appearance, except for their small eyes (Fig. 1C). During development, we examined eye structure in more detail using frozen sections. We first confirmed that Cre was expressed in nearly the whole area of the retina at E17.5 (Fig. 1D), as expected from the expression pattern of Dkk3-Cre original mice.[19] At E16.5, the retinas of the Dicer-CKO mice were already smaller than those of control mice (Figs. 1E, 1F). At this stage, the ganglion cell layer (GCL) was visible in control (Fig. 1E, arrows) but not in the Dicer-CKO (Fig. 1E) mice. At E18.5, the difference between retinal sphere diameters in the Dicer-CKO and littermates became clearer (Figs. 1G, 1H). At P1, the GCL and the inner plexiform layer (IPL) were clearly formed in the control retinas (Fig. 1J) but had not formed in the Dicer-CKO retinas. Retinal diameters were even smaller than those at E16.5 in Dicer-CKO mice, and the cells were not tightly linked (Fig. 1I). At P5, the retina was very thin, and no layered structure was observed in the Dicer-CKO mice (Fig. 1K'). At P14, the retina had no visible structure in Dicer-CKO mice, and there only a few cell aggregates remained in the central region in Dicer-CKO retinas (Fig. 1M).

We measured retinal thickness. Retinas of Dicer-CKO were thinner than those of control mice at E17 and constantly became thinner as development proceeded (Fig. 1O).

Differentiation Markers of Retinal Subtypes Were Once Expressed, Then Disappeared, as Retinal Development Proceeded

To examine the differentiation of retinal subtypes in the Dicer-CKO retina, we immunostained various markers of retinal subtypes using frozen sections. At first, control staining to examine nonspecific signal was performed using frozen, sectioned retinas at E17 and P6. Control immunoglobulin was used as the first antibody, and appropriate second antibodies conjugated with either Alexa 488 or Alexa 594 were stained. With E17 samples, mouse IgG showed nonspecific staining in regions around the GCL and inner nuclear layer (INL), which was thought to be the blood vessel, and rat primary antibody gave no significant nonspecific staining (Supplementary Fig. S1, http://www.iovs.org/lookup/suppl/doi:10.1167/iovs.10-6428/-/DCSupplemental). At P6, signals around GCL in mouse IgG antibodies, but not in the rat IgG antibody, were observed (Supplementary Fig. S1, http://www.iovs.org/lookup/suppl/doi:10.1167/iovs.10-6428/-/DCSupplemental). At E16, although the control retina had no layer structure except for the GCL, the inner half of the cells had became postmitotic whereas the outer half was still composed of undifferentiated progenitor cells, as shown by the restricted expression of the early neural marker βIII-tubulin in the inner half (Fig. 2A). In Dicer-CKO mice, although the βIII-tubulin signal was observed in the inner side of the Dicer-CKO retina, there were also signals in the outer half of the retina; consequently, there was no clear boundary between βIII-tubulin–positive and -negative fields, as seen in the controls (Fig. 2A). Then we examined the expression of differentiation markers. GS, a marker of Müller glia cells, was expressed in the inner half of the retina in controls (Fig. 2A). Again, like the βIII-tubulin staining pattern, GS expression was scattered throughout the Dicer-CKO retina, and no boundary between GS-positive and -negative regions was observed. HuC/D, a marker for amacrine and ganglion cells, and Brn3b, which is expressed in ganglion cells, were expressed in the innermost part of the control retina, forming a layer-like structure (Fig. 2B). In the Dicer-CKO retina, HuC/D was weakly expressed with relatively stronger intensity in the inner half of the retina (Fig. 2B). The Brn3b pattern was also expressed in the inner side, and strong signals were also observed in the outer region (Fig. 2C). Although Brn3-positive cells were seen in the innermost side of the retina, the IPL was not observed, suggesting that process extension is inhibited by the depletion of Dicer. These results indicate that, in Dicer-CKO mice, early differentiation of retinal progenitor cells was under way. We next examined the time course of the expression of several markers. Expression of calbindin, an amacrine and horizontal cell marker, was clearly observed as making lines in the outer region and GCL at E19 in controls (Fig. 2D, blue arrows). In the Dicer-CKO retina, expression of calbindin was observed, but positive cells did not make lines and were scattered in the whole area of the retina (Fig. 2D). At P1, controls showed an expression pattern similar to that at E19, but in Dicer-CKO retina, the expression of calbindin was diminished (Fig. 2D).

Brn3 was expressed in GCL at all examined stages in control retinas. At E17 and E18, Brn3 signals were observed at the innermost side of the retina, and it was also scattered at all areas of the retina. At later stages, the number of positive cells decreased, but signals were observed in all areas of the retina (Fig. 3A). We counted the Brn3-positive cells semiquantitatively, and the cell numbers of Brn3 were slightly fewer in

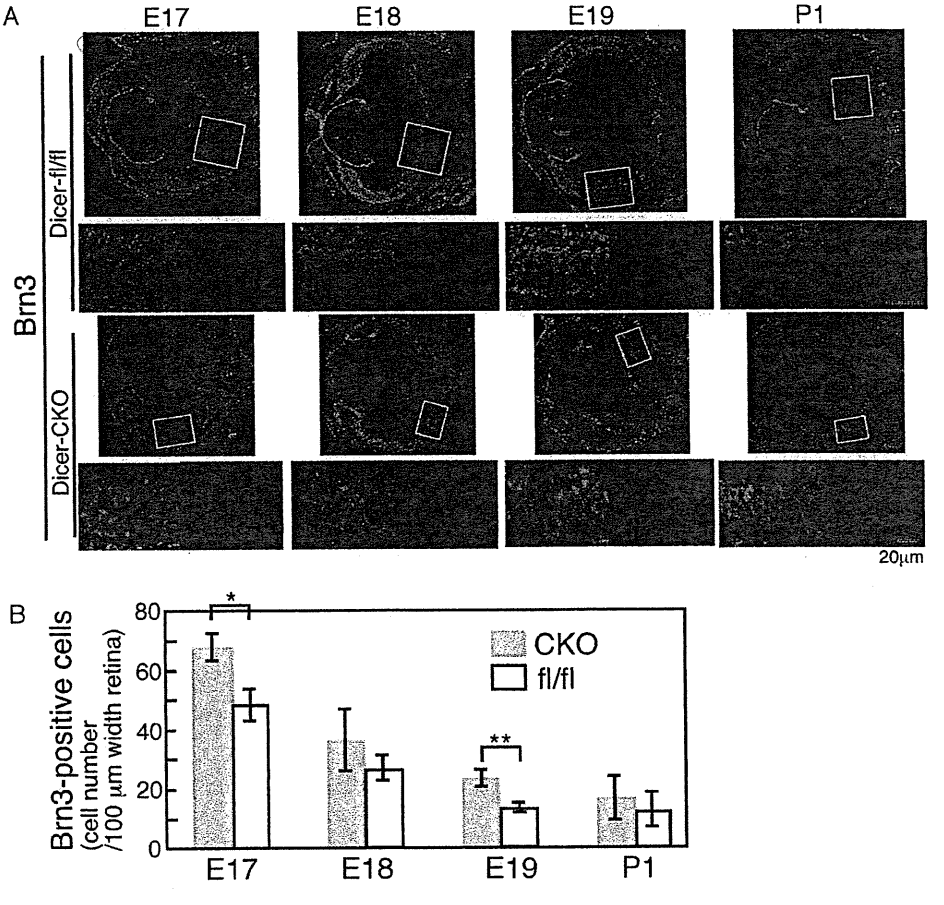

FIGURE 3. Enhanced expression of Brn3 in developing retinas of Dicer-CKO mice. (**A**) Retinas from Dicer-CKO or littermate control mice at indicated stages were frozen sectioned. Immunostaining using anti-Brn3 antibody was performed, and nuclei were visualized by DAPI staining. Scale bars, 100 μm. *Lower* panels are enlarged images of the *white squared regions* in the *upper* panels. (**B**) The number of Brn3-positive cells in the retina at indicated stages was examined. Brn3-positive cells at the central region of the retina were counted under a microscope in an area 100-μm wide. The average of three independent retinas with SD is shown. $^{**}P < 0.01$ and $^{*}P < 0.05$, were calculated by Student's *t*-test.

control than in Dicer-CKO (Fig. 3B) mice. Because the Dicer-CKO retina was thinner than the control retina (data not shown), the percentage of Brn3-positive cells in total retinal cells was much larger in Dicer-CKO than in control. At the P1 stage, Pax6 and PKC were weakly expressed in the whole retinal area (Fig. 4A). GS was not expressed in either control or Dicer-CKO retina, and some PNR-positive cells were observed in the Dicer-CKO retina although no signal was observed in the control retina (Figs. 4A, 4B). At P5, Hu, calbindin, and Pax6 signals were making lines near IPL in the control retina (Fig. 4B). However, in Dicer-CKO, no layer structure was observed even at this stage, but Hu, calbindin, Pax6, and Brn3B expression was observed in the whole retinal area (Fig. 4B).

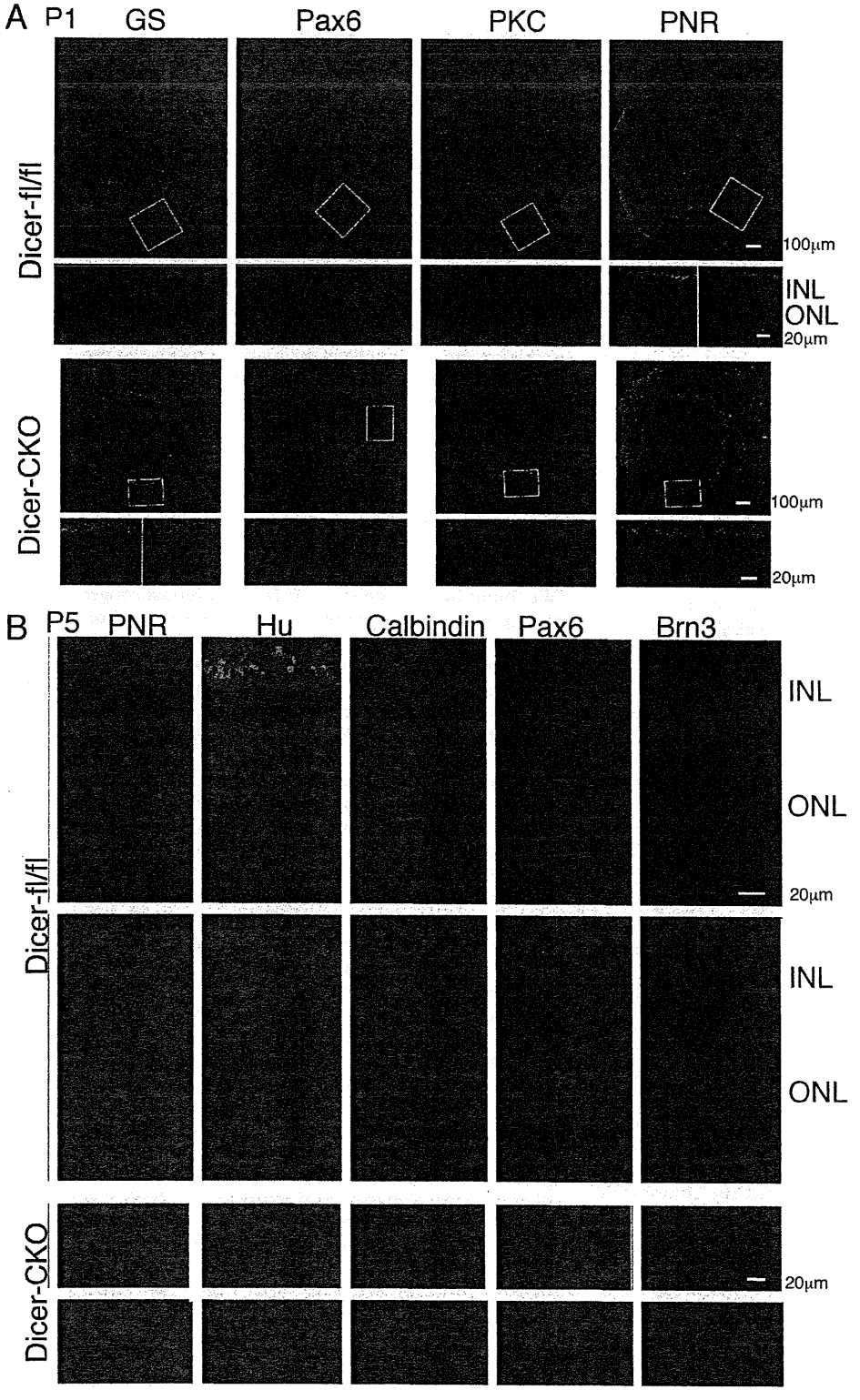

FIGURE 4. Disturbed expression of retinal marker proteins of Dicer-CKO mice after birth. (**A**, **B**) Retinas from dicer-CKO or littermate control mice at P1 (**A**) or P5 (**B**) were frozen sectioned. Immunostaining using indicated antibodies was performed, and nuclei were visualized by staining of DAPI. (**A**) *Lower* panels are enlarged images of the *white squared regions* in the *upper* panels. (**B**) DAPI-stained images. Scale bars are as indicated.

Next, we analyzed cell proliferation by examining anti-phospho-Histone H3, which is a marker of cells at the M phase of the cell cycle. As expected, signals were observed in the most apical edge in both control and Dicer-CKO retinas at E17 (Figs. 5A, 5B). In control samples at E18 and E19, patterns of staining were similar to those at E17 (Fig. 5A). In Dicer-CKO retina, positive signals were observed at the apical-most side, but in some regions, signals were also observed throughout the retinal region (Fig. 5B), suggesting that the layer structure was perturbed in the Dicer-CKO retina. In the P1 control retina, signals had disappeared from some portions of the central region but remained at the periphery (Fig. 5A, P1, inset). In the Dicer-CKO retina, strong signals were still observed in the central region. At P5, signals had completely disappeared from the central region (Fig. 5A, P5, upper panel) but remained in the peripheral region (Fig. 5A, P5, lower panel). In contrast, signals were still observed in both central and peripheral regions in the Dicer-CKO retina (Fig. 5B, P5). Semiquantitative counting of positive cells showed that until P19, the total number of phospho-Histone H3-positive cells was comparable between control and Dicer-CKO retinas (Fig. 5E). At P5, although no signal was observed in the central region of the control retina (Fig. 5A), the total number of phospho-Histone H3 in the control retina was larger than in the Dicer-CKO retina (Fig. 5E), probably because of the small size of the Dicer-CKO retina; this is supported by the finding that the population (%) of phospho-Histone H3-positive cells was bigger in Dicer-CKO than in controls in all examined stages (Fig. 5F). Then we examined cell apoptosis using anti-active caspase3 antibody, which was rarely expressed in any of the examined developmental stages in controls (Fig. 5C, E17~P5) but was strongly expressed in Dicer-CKO retinas at all stages (Fig. 5D, E17~P5), suggesting that abnormal apoptosis was induced in the Dicer-CKO retinas.

Apoptosis Induced by the Deletion of Dicer Is an Autonomous Cell Phenomenon

We examined whether the apoptosis observed in the Dicer-CKO retina was cell autonomous using reaggregation cultures, which are a good model for evaluating the intrinsic characteristics of proliferation and differentiation of donor cells in a defined environment.[23,27] To prepare reaggregation cultures, dissociated retinal cells from Dicer$^{flox/flox}$:GFP $^{+/GFP}$:Dkk3$^{+/cre}$ (Dicer-CKO/GFP) or GFP mice at E16.5 were mixed with an excess number of dissociated host retinal cells from wild-type mice at E16.5. After 5 or 8 days of culture, samples were harvested, frozen-sectioned, and immunostained with anti-GFP antibody. We found that although we used the same number of GFP-positive control or Dicer-CKO/GFP-derived cells in the aggregate cultures, the Dicer-CKO/GFP cells, but not the control GFP cells, decreased quickly during culture. After 8 days of culture, there were fewer than 50 Dicer-CKO cells but a large number of GFP-positive control cells (Fig. 6A). To quantify the results after culturing, we dissociated reaggregations, immunostained the dissociated cells, and counted immunopositive cells semiquantitatively. It was revealed that approximately 25% of Dicer-CKO/GFP cells were active caspase3-positive after 5 and 8 days of culture, whereas fewer than 2% (5 days) or 0% (8 days) of control GFP-positive or -negative cells were positive (Fig. 6B). We also examined the expression of rhodopsin and Pax6; no significant difference in expressing cell populations was observed (Figs. 6C, 6D).

Forced Expression of Cre around Birth Induced Apoptosis and Affected the Expression of Differentiation Markers

To examine the effect of deleting Dicer at a later stage of retinal development, the *Cre* gene was introduced into retinas isolated from Dicer-fl/fl or control mice at P1 using in vitro electroporation. First, we examined the expression of Cre protein by immunostaining frozen sections after 12 days of culture. Strong anti-Cre signals were observed, and most of the signals overlapped GFP signals (Fig. 7A). Apoptosis was also induced by Cre expression in the Dicer-fl/fl retina, but only a very small number of apoptotic cells appeared in the control retina (Fig. 7B). However, we cannot rule out the possibility that the electroporation procedure has a stronger apoptotic effect on Dicer-CKO retinas than on controls. Then we examined the expression of PNR and GS by immunostaining because rod photoreceptors and Müller glia differentiate at a relatively later stage of retinal development. Nearly 90% of the GFP-positive cells were PNR-positive in both control and Dicer-fl/fl retinas (Figs. 7C-E). There were slightly fewer GS-positive cells in control than in Dicer-fl/fl retinas (Figs. 7F, 7I). These results suggest that the differentiation of retinal cells into rod photoreceptors and Müller glia may not be perturbed by the deletion of Dicer. However, when we examined PKC (bipolar) and Islet1 (ganglion and amacrine) markers, we were not able to observe any PKC/EGFP double-positive cells in the Dicer-fl/fl retina (Fig. 7G, 7J). In addition, the number of islet1/EGFP-positive cells in the Dicer/fl/fl retina was significantly lower than in the control retina (Fig. 7H, 7K).

Discussion

We found that the deletion of Dicer in retinal progenitor cells during early development resulted in severe malformation of the retina; before P14, the Dicer-deleted retina had totally degenerated. In the Dicer-CKO retina, caspase was activated at all the examined developmental stages, suggesting that apoptosis was induced by the expression of Cre. Our finding is consistent with a previous study of αPax6-enhancer-dependent Dicer-CKO retinas,[18] reporting increased apoptosis by the deletion of Dicer in retinal progenitor cells. In addition, when we expressed Cre at a later stage (P1), the active caspase signal was observed to be at a significantly higher level than control, suggesting that Dicer is also essential for the survival of retinal cells after birth. This notion is supported by the finding that although some cells expressed differentiation markers and then survived after birth, all the cells ultimately disappeared, and the retina had completely degenerated before P14.

In contrast, retinal differentiation was less affected by the deletion of Dicer. Although localization was perturbed, retinal subtype marker-positive cells were present in the Dicer-CKO retina. In addition, in terms of marker expression, the forced expression of Cre in the later phase of development by electroporation supported the concept of the nonessential role of Dicer in differentiation. However, the detailed examination of marker expression patterns revealed that the effects of deletion of Dicer for each marker are different. The most striking is the upregulation of Brn3. Georgi and Reh[18] also observed a similar phenomenon: the enhanced expression of Brn3 in αPax6-Cre/Dicer-fl/fl mice. They report observing both the upregulation of early neuronal types (such as horizontal cells) and the downregulation of late progenitor cell markers.[18] We examined horizontal cell differentiation by the expression of calbindin, which appeared to be expressed around E19 in the control retina. We did not observe either ectopic expression before E19 or enhanced expression of calbindin in Dicer-CKO retina. In our mice, there was a possibility that the delayed onset of

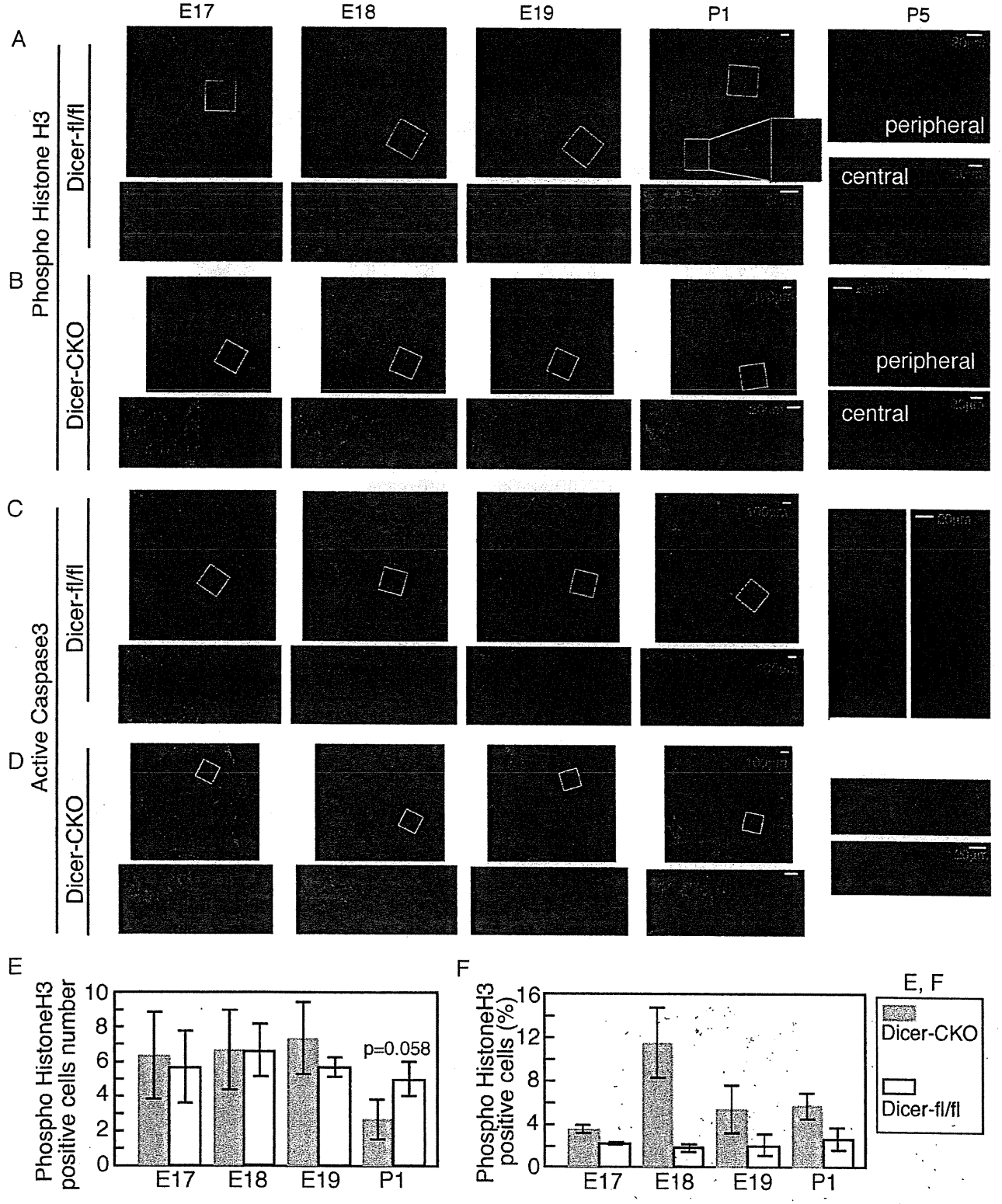

FIGURE 5. Proliferation was slightly suppressed, but massive cell death occurred in Dicer-CKO retinas. Retinas of Dicer-CKO or control Dicer-fl/fl mice at indicated developmental stages were frozen sectioned, and immunostaining was performed using anti-phospho-Histone H3 (**A**, **B**) or anti-active Caspase3 (**C**, **D**) antibodies. Nuclei were visualized by staining with DAPI. (**A**–**D**) E17 to P1. *Lower* panels are enlarged images of the *white squared regions* in the *upper* panels. *Lower right* panels are without DAPI signals. (**A**, **B**) P5. *Upper* panels show peripheral retinas, and *lower* panels show central retinas. (**C**, **D**) P5. Images of the central region of retinas are shown. *Right* panels are without DAPI. (**E**, **F**) Phospho-Histone 3-positive cells in the central region of retina (100-μm wide) were counted at each stage, and the cell number (**E**) and positive cell population in percentages (**F**) are shown. The average of three independent retinas with SD is shown. Scale bars are as indicated.

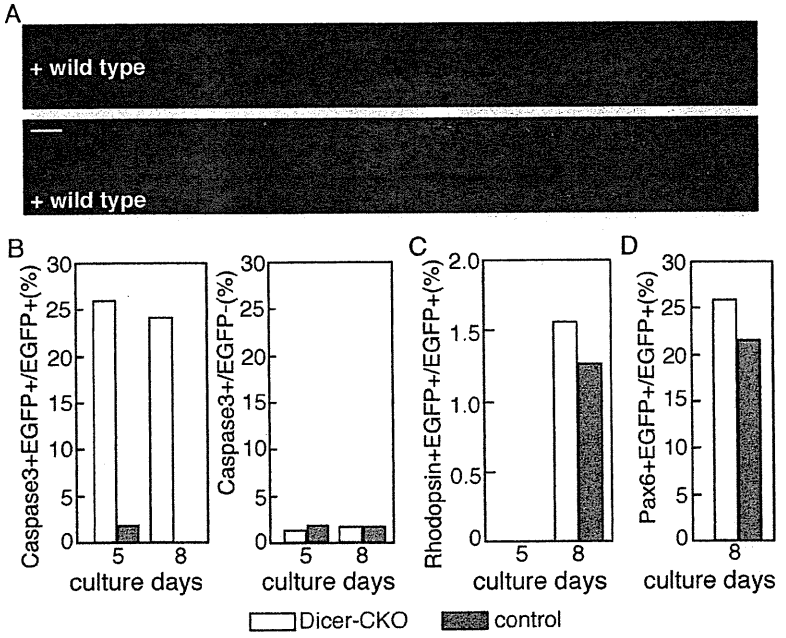

FIGURE 6. Cell death of retinal cells by deletion of Dicer occurred cell autonomously. Re-aggregation culture of retinal cells from Dicer-CKO/GFP or control was performed. Retinal cells at E16.5 were dissociated, mixed with excessively large numbers of host normal cells, and cultured for 12 days. Then re-aggregation cultures were harvested, frozen sectioned, and examined for proliferation and differentiation by immunostaining. (**A**) Sections were immunostained with anti-GFP antibody, and nuclei were visualized by staining of DAPI. Scale bar, 100 μm. (**B–D**) Apoptotic cells (**B**), rhodopsin (**C**)-, and Pax6 (**D**)-positive cells were examined by immunostaining using anti active-caspase3, rhodopsin, and Pax6 antibody, respectively. Double staining with GFP antibody was performed, and marker and EGFP double-positive populations (%) in total EGFP-positive cells are shown. (**B**, *right*) Caspase 3–positive cells in the EGFP-negative population. The same set of experiments was conducted three times, and essentially the same results were obtained.

induction of Cre expression in some retinal progenitor cells might have resulted in their survival, allowing them to differentiate. In the experiments involving Cre expression at the P1 stage, we found a lack of expression of PKC, which is a marker for bipolar cells, and a lower level of Islet1, which is a marker of ganglion and amacrine cells. Taking all our results together, the effects of the deletion of Dicer in retinal progenitor cells might not have been simply a shift of competency of retinal progenitor cells to retinal cells born early. The explanation may be more complex and may depend on the stage of retinal cells. However, given that the lamination of retinal cells had not been observed in any of the differentiation markers, we cannot use information about the subretinal localization of cells to determine whether the expression marker represented fully differentiated retinal cells.

In fact, we observed that the Dicer-CKO retina failed to form laminated retinal structures, and it is difficult to identify which marker-positive cells are equivalent to those in control retinas. Georgi and Reh[18] reported that the formation of GCL and INL was absent. However, Sox2 and Pax6—both retinal progenitor markers—showed relatively normal lamination in the embryonic retina of Dicer-CKO. We observed—at least from E16—no segregation of postmitotic cells or proliferating cells in the Dicer-CKO retina. Among all examinations of immunostaining, only normal positioning of cells was observed in those cells at the M phase that were marked by anti-phospho-Histone H3 antibody. In addition, we observed no layer structure in Dicer mice. In Dicer-CKO mice, the IPL was not clearly observed, suggesting that miRNA regulates the formation process of retinal cells. This suggests that Dicer is less critical for determining the fate of the retina but is critical for the migration and maturation of retinal cells. Taken together, these results show that Dicer is essential to retinal progenitor cell proliferation and survival in the retina during its early development, as in other organs. In addition, even after differentiation, Dicer is essential to cell survival and the final differentiation of retinal cells.

The initial report of retina-specific inactivation of Dicer by Chx10-Cre showed that morphologic defects at P16 progressed to more general cellular disorganization and widespread degeneration of retinal cell types as the animals aged.[17] In this study, the authors stated that the crucial role of Dicer is long-term regulation or retinal cell lamination, survival, and function, with no visible impact on early postnatal retinal structure or function. In our Dicer-CKO mice, at P16, we could not detect any retina-like structure; although some cells remained around the lens, these cells were active caspase3-positive. In contrast, Georgi and Reh[18] and we observed massive cell death at an early stage of retinal development. Because the same Dicer-flox mice[14] were used in the studies, this might have been due to differences in the Cre mice. Damiani et al.[28] used Chx10-Cre mice, made by using a *Chx10*-BAC construct. Chx10-BAC reporter analysis showed that the *Chx10* enhancer drives downstream genes beginning from at least E11.5. However, mosaic expression of target genes in the retina was observed.[28] Mosaic expression of Cre was also observed in Chx10-Cre/Dicer-flox mice.[17] Based on the lack of a severe phenotype, it was surmised that either miRNAs in the retina are extremely stable or that an additional protein can compensate for Dicer function during early postnatal life.[17] Georgi and Reh[18] discussed the possibility of non–cell-autonomous rescue of the phenotype of the Chx10-Cre/Dicer-deficient retina and

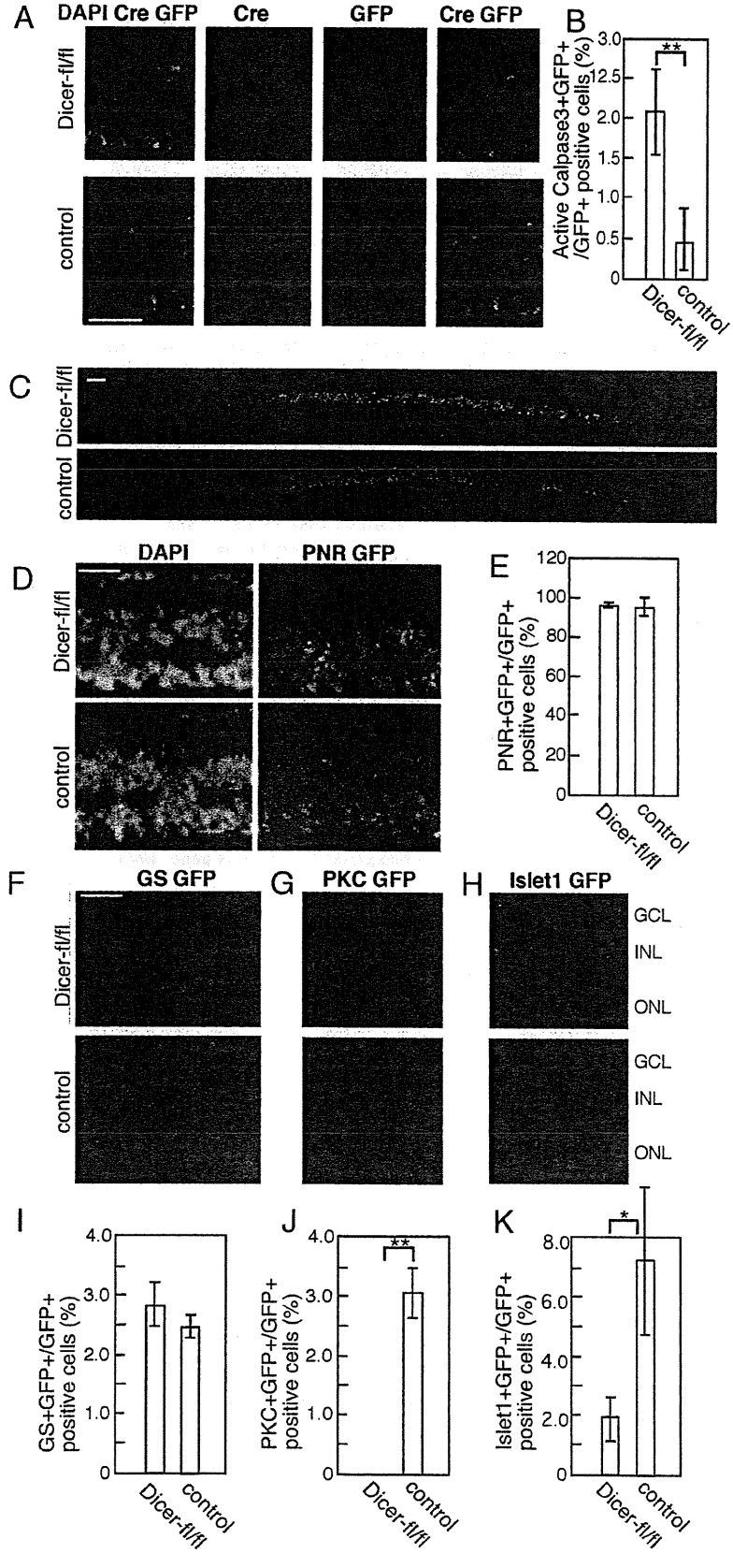

FIGURE 7. Expression of Cre at P1 Dicer-CKO retina resulted in enhanced apoptosis and perturbation of differentiation. (**A**) pCAG-Cre-IRES-EGFP was introduced into the retina at P1 of wild-type mice by electroporation. After 12 days of culture, expression of Cre and EGFP was examined by anti-Cre and -EGFP antibodies, respectively, by immunostaining of frozen sections. Similar results were obtained when we used retinas from Dicer-fl/fl mice. Scale bar, 50 μm. (**B–G**) pCAG-Cre-IRES-EGFP was introduced into retinas at P1 of control (wild-type) or Dicer-CKO and was cultured for 12 days. Apoptosis was examined by anti-active Caspase 3 antibody, and positive cells in the central retinal region (100 μm wide) were counted semiquantitatively in EGFP-positive cells (**B**). Differentiation of cells into photoreceptor (**C–E**), Müller glia (**F**, **I**), bipolar (**G**, **J**), or ganglion/amacrine (**H**, **K**) was examined by immunostaining with anti-PNR, GS, PKC, or Islet1 antibodies, respectively. Populations of PNR (**E**)-, GS (**I**)-, PKC (**J**)-, or Islet1 (**K**)-positive cells in total EGFP-positive cells were calculated semiquantitatively in the central retinal region (100 μm wide). The average of three independent retinas with SD is shown. $^{**}P < 0.01$ and $^{*}P < 0.05$ were calculated by Student's *t*-test. Nuclei were visualized by staining of DAPI. Scale bars: 100 μm (**B**), 50 μm (**C**), 100 μm (**E**), and 50 (**F**) μm.

the difference of onset of Cre in these mice. However, our observation of reaggregation culture suggested that the effects of deletion of Dicer are cell autonomous. The electroporation of Cre-expressing plasmid suggested that the severe effects of Cre deletion may be unrelated to the timing of expression, at least until the neonatal stage. Therefore, we postulated that mosaic expression of Cre is a less likely explanation of the phenotype. Furthermore, it seems unlikely that stable miRNA and other Dicer-like proteins are present in Chx10-Cre/Dicer-deficient retina. One possible reason is that the numbers of retinal progenitor cells expressing Cre may be too small in Chx10-Cre/Dicer-flox mice during early developmental stages and that the elimination of these cells was negligible in comparison with healthy cells or did not affect the gross morphology of the retina during development. Consequently, Chx10-Cre may turn on after birth in bipolar cells and cause the later phenotype.

The ubiquitous expression of Cre in retinal progenitor cells afforded by use of the Dkk3-promoter has enabled clarification of the essential role played by Dicer in retinal development.

Acknowledgments

The authors thank Takahisa Furukawa for providing Dkk3-Cre mice; Robert Whittier, Itsuki Ajioka, Shuji Takada, and Yoko Tabata for discussions and technical advice; Yumiko Ishii and the FACS core laboratory for technical support with sorting; and Dovie Wylie for excellent language assistance.

References

1. Marquardt T, Gruss P. Generating neuronal diversity in the retina: one for nearly all. *Trends Neurosci.* 2002;25:32-38.
2. Cepko CL. The roles of intrinsic and extrinsic cues and bHLH genes in the determination of retinal cell fates. *Curr Opin Neurorbiol.* 1999;9:37-46.
3. Harris WA. Cellular diversification in vertebrate retina. *Curr Opin Genet Dev.* 1997;7:651-658.
4. Inui M, Martello G, Piccolo S. MicroRNA control of signal transduction. *Nat Rev Mol Cell Biol.* 2010;11:252-263.
5. Li X, Jin P. Roles of small regulatory RNAs in determining neuronal identity. *Nat Rev Neurosci.* 2010;11:329-338.
6. Mallanna SK, Rizzino A. Emerging roles of microRNAs in the control of embryonic stem cells and the generation of induced pluripotent stem cells. *Dev Biol.* 2010;344:16-25.
7. Decembrini S, Bressan D, Vignali R, et al. MicroRNAs couple cell fate and developmental timing in retina. *Proc Natl Acad Sci USA.* 2009;106:21179-21184.
8. Conte I, Carrella S, Avellino R, et al. miR-201 is required for lens and retinal development via Meis2 targeting. *Proc Natl Acad Sci USA.* 2010;107:15491-15496.
9. Krol J, Busskamp V, Markiewicz I, et al. Characterizing light-regulated retinal microRNAs reveals rapid turnover as a common property of neuronal microRNAs. *Cell.* 2010;141:618-631.
10. Gregory RI, Chendrimada TP, Schiekhattar R. MicroRNA biogenesis: isolation and characterization of the microprocessor complex. *Methods Mol Biol.* 2006;342:23-47.
11. Wang JY, Medvid R, Melton C, Jaenisch R, Blelloch R. DGCR8 is essential for microRNA biogenesis and silencing of embryonic stem cell self-renewal. *Nat Genet.* 2007;39:380-385.
12. Kanellopoulou C, Muljo SA, Kung AL, et al. Dicer-deficient mouse embryonic stem cells are defective in differentiation and centromeric silencing. *Gene Dev.* 2005;19:489-501.
13. Bernstein E, Kim D-KSY, Carmell MA, et al. Dicer is essential for mouse development. *Nat Genet.* 2003;35.
14. Harfe BD, McManus MT, Mansfield JH, Hornstein E, Tabin CJ. The RNaseII enzyme Dicer is required for morphogenesis but not patterning of the vertebrate limb. *Proc natl Acad Sci USA.* 2005;102:10898-10903.
15. Harris KS, Zhang Z, McManus MT, Harfe BD, Sun X. Dicer function is essential for lung epithelium morphogenesis. *Proc Natl Acad Sci USA.* 2006;2208-2213.
16. Davis TH, Cuellar TL, Koch SM, et al. Conditional loss of Dicer disrupts cellular and tissue morphogenesis in the cortex and hippocampus. *J Neurosci.* 2008;28:4322-4330.
17. Damiani D, Alexander JJ, O'Rourke JR, et al. Dicer inactivation leads to progressive functional and structural degeneration of the mouse retina. *J Neurosci.* 2008;28:4878-4887.
18. Georgi SA, Reh TA. Dicer is required for the transition from early to late progenitor state in the developing mouse retina. *J Neurosci.* 2010;30:4048-4061.
19. Sato S, Inoue T, Terada K, et al. Dkk3-cre bac transgenic mouse line: a tool for highly efficient gene deletion in retinal progenitor cells. *Genesis.* 2007;45:502-507.
20. Okabe M, Ikawa M, Kominami K, Nakanishi T, Nishimune Y. 'Green mice' as a source of ubiquitous green cells. *FEBS Lett.* 1997;407:313-319.
21. Ikawa M, Yamada S, Nakanishi T, Okabe M. Green fluorescent protein (GFP) as a vital marker in mammals. *Curr Top Dev Biol.* 1999;44:1-20.
22. Tabata Y, Ouchi Y, Kamiya H, Manabe T, Arai K, Watanabe S. Retinal fate specification of mouse embryonic stem cells by ectopic expression of Rx/rax, a homeobox gene. *Mol Cell Biol.* 2004;24:4513-4521.
23. Koso H, Ouchi Y, Tabata Y, et al. SSEA-1 marks regionally restricted immature subpopulations of embryonic retinal progenitor cells. *Dev Biol.* 2006;292:265-276.
24. Lin Y, Ouchi Y, Satoh S, Watanabe S. The HMG-transcription factor Sox2 is sufficient for the induction of amacrine cells in mouse retina. *Invest Ophthalmol Vis Sci.* 2008;50:68-74.
25. Muto A, Iida A, Satoh S, Watanabe S. The group E Sox8 and Sox9 are regulated by Notch signaling and are required for Muller glial cell development in mouse retina. *Exp Eye Res.* 2009;89:549-558.
26. Matsuda T, Cepko CL. Electroporation and RNA interference in the rodent retina in vivo and in vitro. *Proc Natl Acad Sci USA.* 2004;101:16-22.
27. Belliveau MJ, Cepko CL. Extrinsic and intrinsic factors control the genesis of amacrine and cone cells in the rat retina. *Development.* 1999;126:555-566.
28. Rowan S, Cepko CL. Genetic analysis of the homeodomain transcription factor Chx10 in the retina using a novel multifunctional BAC transgenic mouse reporter. *Dev Biol.* 2004;271:388-402.

INTERNAL MEDICINE

□ ORIGINAL ARTICLE □

Clinical Features of Lymphangioleiomyomatosis Complicated by Renal Angiomyolipomas

Yoshiko Mizushina, Masashi Bando, Tatsuya Hosono, Naoko Mato, Takakiyo Nakaya, Yoshikazu Ishii, Hideaki Yamasawa and Yukihiko Sugiyama

Abstract

Objective Renal angiomyolipomas (R-AMLs) are major complications of lymphangioleiomyomatosis (LAM). The objective of this study was to better understand the influence of R-AMLs in patients with LAM on the prognosis and other clinical factors related to respiration, and to investigate the management of R-AMLs in patients with LAM.

Patients and Methods We retrospectively investigated the clinical features of 7 patients with LAM [4 were TSC (Tuberous sclerosis complex)-LAM and 3 were S (sporadic)-LAM] complicated by R-AMLs admitted to our hospital from 1997 to 2008.

Results All patients were females and the mean age at diagnosis of LAM was 40.7 years (31.7 years for TSC-LAM and 52.7 years for S-LAM). Although 5 patients had symptoms related to R-AMLs, only 1 patient experienced symptoms related to R-AMLs at the time of diagnosis. Five patients had bilateral and 2 patients had unilateral R-AMLs. R-AMLs ruptured in 4 cases (3 patients were TSC-LAM) including 2 patients in whom they ruptured bilaterally, and who underwent bilateral nephrectomy. In 1 case, unilateral R-AMLs grew larger and appeared on the other side during the follow-up period.

Conclusion Although only rare cases of LAM show symptoms related to R-AMLs initially, R-AMLs are a notable complication. To avoid nephrectomy, R-AMLs should be diagnosed when they are small and should be followed up carefully by periodic echograms or CT scans.

Key words: lymphangioleiomyomatosis, renal angiomyolipoma, tuberous sclerosis complex, total nephrectomy

(Intern Med 50: 285-289, 2011)
(DOI: 10.2169/internalmedicine.50.3558)

Introduction

Lymphangioleiomyomatosis (LAM) is a rare disease that occurs predominantly in females and is characterized by the proliferation of smooth muscle cells and cyst formation. LAM occurs in 30% of patients with tuberous sclerosis complex (TSC), but patients with LAM complicated by TSC (TSC-LAM) constitute only approximately 15% of all LAM cases. The remaining cases are sporadic LAM (S-LAM). LAM patients have renal angiomyolipomas (R-AMLs) in about 93% of TSC-LAM and about 30-50% of S-LAM cases (1).

In order to better understand the influence of R-AMLs in patients with LAM on the prognosis and other clinical factors related to respiration, and to investigate the management of R-AMLs in patients with LAM, we retrospectively investigated 7 cases of LAM complicated by R-AMLs who were admitted to our hospital from 1997 to 2008.

Patients and Methods

Thirteen patients with LAM were admitted to our hospital from 1977 to 2008. We investigated the clinical features of 7 patients with LAM (4 were TSC-LAM and 3 were S-LAM) complicated by R-AMLs. Retrospective chart reviews were performed on each case. The size of the R-AMLs were measured from echograms or computed tomography (CT)

Division of Pulmonary Medicine, Department of Medicine, Jichi Medical University, Japan
Received for publication February 18, 2010; Accepted for publication October 11, 2010
Correspondence to Dr. Yoshiko Mizushina, mizushina@jichi.ac.jp

Table 1. Clinical Characteristics of 13 LAM Cases

Case No.	Age of diagnosis as LAM*1	Age of initial symto-ms	R-AMLs *2	TSC *3	Initial symtoms	Symptoms of R-AMLs	Pneumo-thorax	Duration until induction of HOT*4 from initial symptoms[years]	Decline of VC*5/year[ml]	Decline of $FEV_{1.0}$*6/ year[ml]	Therapy	Follow up period from diagnosis	Respiratory failure
1	32	27	+	-	Chest pain	Abdominal pain	+	-			progesteron	26 years	-
2	58	50	+	-	Dyspnea on exertion	Abdominal pain	+	11	12.86	51.43		Induction of IPPV for respiratory failure after 9 years	+
3	42	41	+	-	Dyspnea on exertion	-	-	13	1.54	52.31	progesteron	Progression of respiratory failure Transfer to another hospital after 16 years	+
4	34	32	+	+	Dyspnea on exertion	Abdominal pain and lumbago	+	3	136.67	79.17	progesteron	Progression of respiratory failure 14 years	+
5	29	29	+	+	Cough and fever	Appetite loss and nausea	-	-	-5.00	-21.67		Induction of hemodialysis 15 years	-
6	58	30	+	-	Pneumothorax	-	+	2				Dead of respiratory failure after 2 years Diagnosed by autopsy	+
7	32	31	+	+	Abdominal distention	Abdominal distention	+	-				2 years Renal transplantation was performed	-
8	42	39	-	-	Hemosputum		+	-	25.00	24.29		Progression of respiratory failure Dead of breast cancer after 17 years	+
9	46	40	-	-	Dyspnea on exertion		-	-				Dead of respiratory failure after 2 years Diagnosed by autopsy	+
10	38	37	-	-	Back pain		+	-	41.88	42.50		17 years	-
11	33	32	-	-	Cough and sputum		-	5	58.89	26.67	Progesteron +ovariectomy	Induction of IPPV for respiratory failure after 14 years	+
12	29	29	-	-	Cough and fever		-	-			progesteron	Drainage of chylothorax Transfer to another hospital after a year	-
13	29	27	-	-	Cough and lumbago		-	2	477.50	137.50	Progesteron LH-RH analog, Lung transplantation	Lung transplantation was performed after 3 years 3 years after transplantation	+

*1 LAM; Lymphangioleiomyomatosis, *2 R-AML; renal angiomyolipoma, *3 TSC; Tuberous sclerosis complex
*4 HOT; Home oxygen therapy, *5 VC; Vital capacity, *6 $FEV_{1.0}$; Forced expiratory volume in 1 second,

scans.

We diagnosed LAM using the diagnostic criteria established by the Respiratory Failure Research Group of the Japanese Ministry of Health, Labour and Welfare in 2005 (2).

We diagnosed R-AMLs based on echograms or CT scans. The appearance of R-AMLs on echogram is a strongly hyper-reflective lesion with acoustic shadowing. This appearance is a result of the multiple tissue interfaces between fatty and non-fatty components of the mass. The appearance of R-AMLs on unenhanced CT scan is a predominantly fatty inhomogeneous mass with varying amounts of tissue density interspersed within it. Minimal fat AMLs which contain only microscopically detectable fat account for 4.5% of R-AMLs. Although it is difficult to diagnose minimal fat AMLs by their appearance on echogram or CT scan, homogeneous enhancement and a prolonged enhancement pattern on CT scan are the most accurate predictors (3).

A statistical software package (Dr.SPSS II, for Windows; SPSS Inc.) was used for the analysis. Results are presented as the mean±standard error of the mean (SEM). The differences between the two groups were compared using Student's unpaired t-test. Fisher's exact test was calculated to assess relationships between the two parameters. A value of $p<0.05$ was considered statistically significant.

Case 7 was previously reported in 2008 in *Urology* (4).

Results

All of the patients were females and the mean age at diagnosis of LAM was 40.7 years. Seven cases were complicated by R-AMLs (Table 1).

All 4 patients (100%) with TSC-LAM had R-AMLs. Three of 9 patients (33%) with S-LAM had R-AMLs. The mean ages of patients at diagnosis of LAM with R-AMLs were 31.7 years for TSC-LAM patients and 52.7 years for S-LAM patients (Table 1). There were no significant differences between the groups with and without R-AMLs in the rates of pneumothorax ($p=0.21$) or respiratory failure ($p=0.63$).

Five patients had bilateral and 2 patients had unilateral R-AMLs. R-AMLs ruptured in 4 cases (3 patients were TSC-LAM), including 2 patients in whom they ruptured bilaterally. Renal artery embolization had been performed in 1 case, nephrectomy had been performed in 4 cases, and bilateral nephrectomy had been performed in the 2 cases with bilateral rupture (Table 2). Regarding changes in R-AMLs during the follow-up period, in 1 case (Case 1), unilateral R-AMLs grew larger (3 cm to 4 cm in 2 years) and appeared on the other side as well (Table 2). Four patients had hepatic angiomyolipomas and R-AMLs (3 were S-LAM and 1 was TSC-LAM) (Table 2).